Received: 13 June 2019 | Revised: 12 September 2019 | Accepted: 14 September 2019

DOI: 10.1002/aoc.5283

WILEY Applied Organometallic Chemistry

FULL PAPER

Organotin(IV) complexes of NSAID, ibuprofen, X-ray structure of $Ph_3Sn(IBF)$, binding and cleavage interaction with DNA and *in vitro* cytotoxic studies of several organotin complexes of drugs

Ranjana Kumari[1] | **Somesh Banerjee**[2] | **Partha Roy**[2] | **Mala Nath**[1]

[1] Department of Chemistry, Indian Institute of Technology Roorkee, Roorkee 247667, India

[2] Department of Biotechnology, Indian Institute of Technology Roorkee, Roorkee 247667, India

Correspondence
Mala Nath, Department of Chemistry, Indian Institute of Technology Roorkee, Roorkee 247667, India.
Email: malanfcy@iitr.ernet.in; malanfcy@gmail.com

Funding information
Ministry of Human Resource Development, Grant/Award Number: Grant No. MHRD -02-23-104-429; Ministry of Human Resources Development, Grant/Award Number: MHRD -02-23-104-429

This study encompasses the synthesis and characterization of organotin(IV) derivatives of non-steroidal anti-inflammatory drug ibuprofen (IBF), *viz.* $[(Me_3Sn)(IBF)]$ (**1**), $[(Bu_3Sn)(IBF)]$ (**2**), $[Ph_3Sn(IBF)]$ (**3**), $\{[Me_2Sn(IBF)]_2O\}_2$ (**4**) and $[Bu_2Sn(IBF)_2]$ (**5**). The crystal structure of complex **3**, $[Ph_3Sn(IBF)]$, indicates a highly distorted tetrahedral (td) geometry with anisobidentate mode of coordination of the carboxylate group with tin atom, and a similar structure has been proposed for other two triorganotin(IV) derivatives. Moreover, the DFT (density functional theory) calculation and other studies have verified a dimer distannoxane type of structure for complex **4**, $\{[Me_2Sn(IBF)]_2O\}_2$. Complex **5** has been found to exhibit a highly distorted octahedral geometry around the tin atom. To investigate the DNA binding profile of the synthesized complexes, viscosity measurement, UV–vis and fluorescence titrations were performed, which revealed an intercalative type of binding with DNA for IBF and complex **5** and external binding in case of the complexes **1** and **2**; complexes **3** and **4** could not be studied owing to their insufficient solubility in tris buffer. Plasmid DNA fragmentation studies of IBF and complexes **1**, **2** and **5** indicate that they cleaved the pBR322 plasmid potentially. Further, the drugs IBF {2-[4-(2-methylpropyl)phenyl]propanoic acid}, MESNA (sodium 2-mercaptoethane-sulfonate), warfarin [2H-1-benzopyran-2-one,4-hydroxy-3-(3-oxo-1-phenylbutyl)], sulindac (2-{5-fluoro-1-[(4-methanesulfinylphenyl) methylidene]-2-methyl-1H-inden-3-yl}acetic acid) and their corresponding organotin(IV) complexes **1–19** (complexes **6–19** were synthesized/reported previously) were screened *in vitro* for cytotoxicity against human cancer cell lines *viz.* DU145 (prostate cancer), HCT-15 (colon adenocarcinoma), Caco-2 (colorectal adenocarcinoma), MCF-7 (mammary cancer), LNCaP (androgen-sensitive prostate adenocarcinoma) and HeLa (cervical cancer), through MTT reduction assay and the cause of cell death was investigated through acridine orange/ethidium bromide staining of cells and DNA fragmentation assay. The probable structure–cytotoxicity relationship is also discussed. The major role of apoptosis along with small necrosis was also validated by flow cytometry

assay using annexin V–fluorescein isothiocyanate and propidium iodide analysis.

KEYWORDS

apoptosis, cytotoxicity, DNA binding, organotin(IV) complexes of drugs, plasmid cleavage

1 | INTRODUCTION

It has been reported in the literature that several non-steroidal anti-inflammatory drugs (NSAIDs) play a crucial role in suppressing tumor activities[1–3] and can also be used as effective modulators in combination therapies with anticancer drugs, *viz.* cyclophosphamide, melphalanor and carmustine.[4] Endo et al. suggested that ibuprofen (IBF) is a potential chemotherapeutic agent which might allow lower doses of *cis*-platin and may limit the challenges associated with its side effects and the development of resistance, by the down-regulation of Hsp70, which is a contributor to the process of tumor generation.[3] Ibuprofen is an NSAID and has been shown to cure cancers of the colon, protostate, lung and breast.[5,6] Few literature reports have discussed the DNA binding capacities of aspirin and IBF,[7,8] which might be responsible for their cytotoxicities. Complexes of IBF with different metals have been found to exhibit significant antimicrobial and antitumor activities.[9–13] Ruthenium and copper complexes of IBF possess sufficient antitumor activities *in vitro* against mouse mammary (EMT6), human breast (MDA-MB-231), human prostate (DU145), human skin melanoma (HT-144) and SKMEl-28 cancer cell lines.[12,13] Few organotin complexes of IBF have been reported to show good antibacterial activities; however none of them was studied for their DNA binding capacity and antitumor activities.

Utilization of platinum-based compounds as antitumor drugs has ignited new wave of interest in the synthesis and testing of new metal complexes as antitumor agents. However, the side effects, toxicity and drug resistance associated with platinum-based compounds have led many researchers to look for new alternatives with higher potency towards platinum-resistant cancer cells with fewer side effects. The organotin carboxylates can be regarded as the best substitute for platinum-based antitumor drugs owing to their extensive structural possibilities and wide range of biological activities, especially their high *in vivo* and *in vitro* antitumor activities.[14,15] Taking into account the importance of non-steroidal anti-inflammatory drugs (NSAIDs) and complexes of drugs with organotin moieties, this study deals with the synthesis and characterization of five complexes of organotin (IV) moieties with IBF. Since the organotin complexes were designed to imitate platinum-based drugs, the function of these complexes was presumed to be based on interaction with DNA, which is regarded as one of the major targets for anticancer candidates.[16–19] Therefore, the DNA-binding profiles of synthesized complexes, **1**, **2** and **5** have been investigated through various biophysical techniques and the plasmid–DNA cleavage pattern has been investigated using gel electrophoresis technique. However, the DNA-binding and cleavage profiles for drugs, MESNA, sulindac (SUL), warfarin (WR) and their respective organotin complexes, **6–19**, have recently been reported by us.[20–22] In order to correlate the DNA binding and cleavage potential with cytotoxic effect exerted by the different drugs and their corresponding organotin (IV) complexes, and to explore the comparative accounts of the structure–activity relationships of different drugs and complexes **1–19**, their *in vitro* cytotoxicity (MTT assays) has been investigated against some selected cell lines, *viz.* DU145 (prostate cancer), HCT-15 (colon adenocarcinoma), Caco-2 (colorectal adenocarcinoma), MCF-7 (mammary cancer), LNCaP (androgen-sensitive prostate adenocarcinoma) and HeLa (cervical cancer). Further, the underlying cause of cell death was examined through acridine orange (AO)/ethidium bromide (EB) staining of cancer cell lines and DNA fragmentation assay. In order to ascertain more information about their mode of action, a flow cytometry assay using annexin V–fluorescein isothiocyanate and propidium iodide was also carried out.

2 | EXPERIMENTAL SECTION

Details of all reagents, materials, methods and instruments used are described in the Supporting Information. The colourless and rectangular block-shaped crystals of complex **3** [(Ph_3Sn(IBF)] were obtained with very slow evaporation of solvent (chloroform) from the concentrated complex solution filled in a glass tube of small diameter and left undisturbed at ambient temperature for 5 days. Single-crystal X-ray diffraction data at ambient temperature was acquired by mounting a suitable crystal of Ph_3Sn(IBF) ($0.25 \times 0.20 \times 0.17$) mm on a Bruker Kappa Apex-II charge-coupled device detector diffractometer having a graphite monochromated Mo Kα radiation ($\lambda = 0.71073$ Å) source at the Institute Instrumentation

Centre, Indian Institute of Technology Roorkee, Roorkee, India. The crystal structure was solved by processing the diffraction data using the 'direct method' with SIR-92 program[23] and all non-hydrogen atoms were refined anisotropically by applying 'Full matrix least-squares calculations based on F2' using the SHELXL97 program.[24] All hydrogen atoms were located and were rendered to ride on their respective parent atoms. An illustrative ORTEP diagram for the molecular structure (as shown in Fig. 1) of complex **3** (CCDC ID-1814179) along with the schematic non-hydrogen atom labelling was developed using Mercury version 4.1.0 software.

2.1 | DNA binding studies of complexes 1-5

To elucidate the mode and extent of binding of IBF/studied complexes towards DNA, biophysical studies were carried out by preparing an appropriate dilution of stock solution (in DMSO) of complexes in Tris–HCl/NaCl buffer (pH 7.2, 5:50 mM), so that the final dilution contained no more than 1% DMSO. Complex **3** [Ph_3Sn(IBF)] is insoluble and complex **4**, $[(Me_2Sn–IBF)_2O]_2$ is partially soluble in tris buffer, hence DNA binding studies of these complexes could not be performed. Freshly prepared dilutions of remaining complexes were used. CT DNA (calf thymus DNA) stock solution once prepared was not used after 2 days.

2.1.1 | UV–vis spectrophotometric titration

The UV–vis spectra of IBF and complexes (**1**, **2** and **5**; 6.7×10^{-5} M) were recorded in the absence and presence of CT DNA (calf thymus DNA). Absorbance (A) of IBF and complexes **1**, **2** and **5** was obtained with successive addition of CT DNA (0.6–15 μM) while keeping total volume constant. In order to eliminate the absorbance owing to CT DNA the reference solution was maintained at equal concentration of CT DNA to that of working solution. As the data does not fit the linear regression model when plotted as $[DNA]/(\epsilon_a - \epsilon_f)$ vs [DNA] (where [DNA] is the concentration of CT DNA, ϵ_a is the apparent extinction coefficient and ϵ_f corresponds to the extinction coefficient of the metal complexes in free form), thus the intrinsic binding constant K_b (equal to slope to intercept ratio) could not be determined, and further, fluorescence studies were employed to estimate the extent of binding.

2.1.2 | Fluorescence titration and viscosity measurement studies

All of the fluorescence emission experiments were carried out by diluting stock solution of the complexes, prepared in 1% DMSO with Tris–HCl/NaCl buffer (pH = 7.2) at 25 °C. IBF and complexes (**1**, **2** and **5**) were excited at 264 nm. Emission spectra were recorded in the range 270–360 nm with maximum emission at 290 nm. The DNA binding experiment was carried out by recording the emission spectra of IBF/complexes (6.7×10^{-5} M) alone and with increasing concentrations (2–20 μM) of CT DNA. In the EB displacement experiment, the emission spectra of a pre-incubated solution of CT DNA (20 μM) and EB (5 μM) in the absence and presence of increasing concentrations of IBF and complexes (2–20 μM) were recorded. The EB–CT DNA adduct ([DNA]/[EB] = 4) was excited at 515 nm and emission spectra were

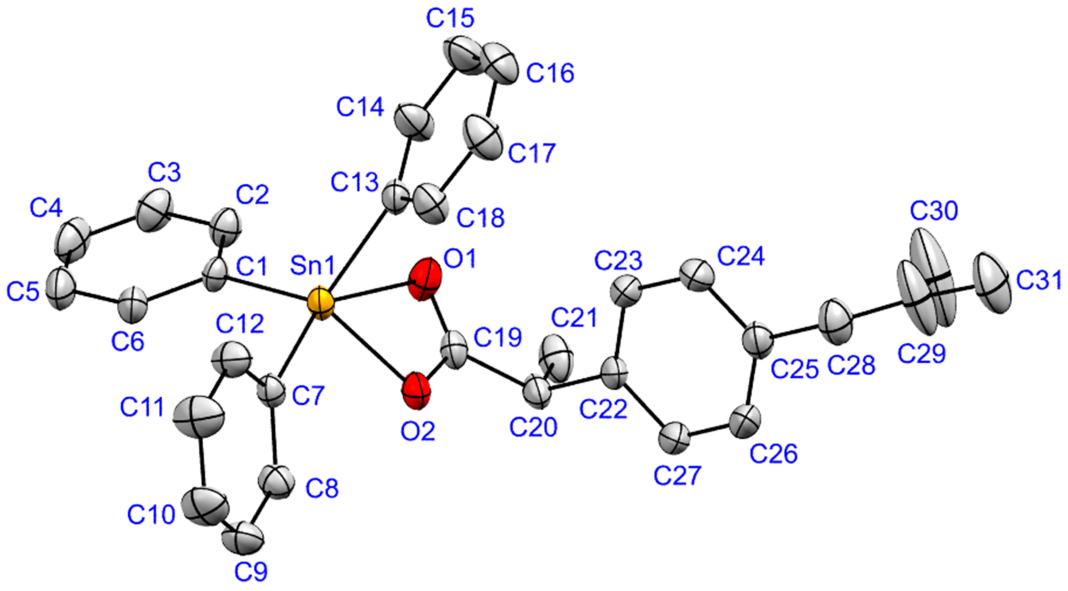

FIGURE 1 ORTEP diagram of Ph_3Sn(ibuprofen, IBF) at thermal ellipsoids (50% probability); H-atoms are omitted for clarity

observed in the range 525–700 nm with a slit width of 2 nm. In another experiment iodide quenching was studied in which emission spectra of complexes (6.7×10^{-5} M) were recorded in the absence and presence of CT DNA (20 μM) with subsequent addition of KI (potassium iodide) (0–72 mM). Stern–Volmer quenching constants K_{sv} in both the quenching experiments were evaluated[20–22] using the classical Stern–Volmer equation. Viscosity of CT DNA (100 μM) was measured in the presence and absence of IBF/complexes (**1**, **2** and **5**; 20–100 μM) in Tris–HCl/NaCl buffer (pH = 7.2) at 25 °C.

2.2 | DNA cleavage and gel electrophoresis

The DNA cleavage study was performed using supercoiled pBR322, *Escherichia coli* plasmid DNA. The supercoiled DNA (100 ng) was treated with varying concentrations of IBF and complexes (20–80 μM) with and without activators or radical quenchers in buffer solution (5:50 mM Tris–HCl/NaCl, pH 7.2) and were incubated for 5 h at 37 °C. Incubated samples were then treated with 2 μL loading buffer [30 mM EDTA, 0.05 % (w/v) glycerol, 36% (v/v) bromophenol blue] and loaded onto agarose gel (0.8%) containing EB (0.5 μg/mL). The agarose gel was run in 0.5 × TBE buffer at 50 V/cm for 3.5 h. Bands formed by moving plasmid DNA were visualized and photographed using a gel documentation system (Bio-Rad, USA).

2.3 | Flow cytometry for analysis of apoptosis

The pattern of cell death in response to the treatment drug, flow cytometry was performed using Annexin V–fluorescein isothiocyanate and propidium iodide.[25,26] Briefly, 1×10^6 cancer cells were seeded in six-well plates. The cells were maintained in DMEM media and incubated at 37 °C for 24 h in a humidified, 5% CO_2 incubator. After this, the cells were incubated with different complexes for another 24h. Vehicle (DMSO: dimethylsulfoxide) treated cells were incubated as control cells. After this, the cells were collected and harvested for processing according to the manufacturer's protocol (Alexa Fluor® 488 Annexin V/Dead Cell Apoptosis Kit, Invitrogen, USA). After the incubation in dark was over, the cells were immediately analysed by FACS Verse flow cytometer (BD Biosciences) to avoid fluorescence quenching. The data were analysed using BD FACSuite software (BD Biosciences).

Detailed experimental procedures of the cytotoxic study through MTT assay, acridine orange/ethidium bromide staining and DNA fragmentation assays were followed as reported previously[26] and are also given in the Supporting Information.

2.4 | Synthesis

Complexes of triorganotin(IV) and dimethyltin(IV) with IBF (complexes **1–4**) were synthesized through the thermal method by preparing sodium salt of IBF *in situ*, and dibutyltin(IV)–IBF complex (**5**) was synthesized by the microwave method. Syntheses of complexes **6–19** was previously reported.[20–22]

2.4.1 | Synthesis of triorganotin(IV)–IBF complexes (1–3)

Sodium salt of IBF was prepared by stirring the solution of IBF (5 mM, 1.04 g) in 75 mL methanol and sodium methoxide, which was prepared by reacting sodium metal (5.5 mM, 0.126 g) in 15 mL of dry methanol for 4 h at ambient temperature. The resulting solution was then evaporated, washed and dried, and preserved for further synthesis of complexes. To a solution of sodium salt of IBF (0.5 mmol, 0.115 g) in 15 mL of specially dried methanol, a hot methanolic (15 mL) solution of trimethyltin (IV) chloride (0.5 mmol, 0.100 g), triphenyltin(IV) chloride (0.5 mmol, 0.193 g) or tributyltin(IV) chloride (0.5 mmol, 0.141 mL) was added. The solution thus formed was refluxed with continuous stirring for 4 h. The reaction mixture was continuously supplied with dry nitrogen. The excess solvent was evaporated under reduced pressure. The products thus obtained were washed with a mixture of methanol and *n*-hexane (1:3, v/v), dried under vacuum and weighed.

2.4.2 | Synthesis of dimethyltin(IV)–IBF complex (4)

To a mixture of Me_2SnCl_2 (0.5 mmol, 0.110 g) and IBF (0.5 mmol, 0.103 g) in 30 mL of specially dried methanol, NaOH (2M, 1 mL) was added and the resulting solution was refluxed for 2 h. Further, 3 g of Na_2SO_4 was added in the solution and again refluxed for 4 h. The solution was kept for 2 days at ambient temperature and product started to separate out, which was then filtered and washed with methanol and *n*-hexane (1:1, v/v), and dried under vacuum and weighed.

2.4.3 | Synthesis of dibutyltin(IV)–IBF complex (5) by the microwave-assisted method

Microwave-assisted syntheses were carried out in an open glass vessel microwave oven (Magicook 20S (Galaxy) Whirlpool) with a rotating tray and having maximum

microwave energy output of 800 W. In order to synthesize complex **5**, IBF (1 mmol, 0.206 g) and dibutyltin oxide (0.5 mmol, 0.124 g) were finely ground together to obtain a homogeneous mixture. A paste of this mixture was made by adding few drops of methanol and irradiated for 1 min in a microwave oven at 400 W, in a Petri dish. The reaction mixture was then allowed to cool at room temperature and again irradiated for 1 min; this process was repeated 4 times. An oily compound appeared in the Petri dish, which was dried after triturating with hexane several times. The resulting product was scratched and washed with *n*-hexane and dried in vacuum.

2.4.4 | Attempted syntheses

Syntheses of dioctyltin(IV) and diphenyltin(IV) complexes with IBF were also tried through microwave and thermal methods, but in both the cases an oily mass was obtained which was a mixture of product and reactants, which could not be purified. Furthermore, efforts to synthesize the mixed ligand complexes of organotin (IV) with IBF and 1,10-phenanthroline were made, but were not successful.

2.4.5 | IBF, $C_{13}H_{18}O_2$

Physical state: white solid; m.p.: 79 °C; MW = 206.2; IR (KBr, cm^{-1}): ν (OH) 2500–3300 (br), ν(C=O) 1707(s), ν(C=C)/ν (ring) 1636(m) 1563(s), 1465(s); ^{1}H NMR [δ (ppm), $CDCl_3$, 399.78 MHz]: 3.72 (q, 1H, H-2), 1.51 (d, 3H, H-3), 7.23 (d, 2H, H-5, 5′), 7.11 (d, 2H, H-6, 6′), 2.46 (d, 2H, H-8), 1.85 (m, 1H, H-9), 0.91 (d, 6H, H-10, 10′); ^{13}C NMR [δ (ppm), $CDCl_3$, 100.53 MHz]: 180.03 (C-1), 45.02 (C-2), 18.04 (C-3), 136.93 (C-4), 127.26 (C-5, 5′), 129.38 (C-6, 6′), 140.83 (C-7), 44.95 (C-8), 30.15 (C-9), 22.38 (C-10, 10′).

2.4.6 | $(Me_3Sn)(IBF)$, $C_{16}H_{26}O_2Sn$

Physical state: off-white, solid; yield: 80%, m.p.: 144 °C; MW= 370.1; Anal. calcd for $C_{16}H_{26}O_2Sn$: C 52.09, H 7.10, Sn 32.16; observed: C 51.67, H 6.93, Sn 31.69. IR (KBr, cm^{-1}): ν_{as} (C=O) 1577(s), ν_s(C=O) 1400(s),1359 (m), ν = 186 cm^{-1}, ν(C=C)/ν (ring) 1560(s), 1506(m), 1453(m), ν_{as} (Sn–C)/ν_s (Sn–C) 615(m), 597 (w), ν (Sn–O) 547(s); ^{1}H NMR [δ (ppm), $CDCl_3$, 399.78 MHz]: 3.69 (q, 1H, H-2), 1.45 (d, 3H, H-3), 7.20 (d, 2H, H-5, 5′), 7.07 (d, 2H, H-6, 6′), 2.46 (d, 2H, H-8), 1.84 (m, 1H, H-9), 0.89 (d, 6H, H-10, 10′), 0.50 (9H, H-α), [^2J (^{119}Sn–^{1}H) = 57.6 Hz]; [∠C–Sn–C= 110.8°][b]; ^{13}C NMR [δ (ppm), $CDCl_3$, 100.53 MHz]: 180.28 (C-1), 45.73 (C-2), 19.50 (C-3), 139.18 (C-4), 127.06 (C-5, 5′), 129.12 (C-6, 6′), 139.95 (C-7), 45.04 (C-8), 30.14 (C-9), 22.37 (C-10, 10′), –2.49 (C-α), [^1J (^{119}Sn–^{13}C) = 388 Hz], [∠C–Sn–C= 110.8][c]; ^{119}Sn NMR [δ (ppm), $CDCl_3$, 186.50 MHz]: 136.16.

2.4.7 | $(Bu_3Sn)(IBF)$, $C_{25}H_{34}O_2Sn$

Physical state: white, solid; yield: 83%, m.p.: 52 °C; MW = 496.2; Anal. calcd for $C_{25}H_{34}O_2Sn$: C 60.62, H 8.59, Sn 23.97; observed: C 60.28, H 8.44, Sn 23.11; IR (KBr, cm^{-1}): ν_{as}(C=O) 1586(s), ν_s(C=O) 1391(s), 1356(m), ν = 218 cm^{-1}, ν(C=C)/ν (ring) 1507(s), 1453(m), ν_{as} (Sn–C)/ν_s (Sn–C) 597(m), 511 (w), ν (Sn–O) 544(m); ^{1}H NMR [δ (ppm), $CDCl_3$, 399.78 MHz]: 3.69 (q, 1H, H-2), 1.46 (d, 3H, H-3), 7.22 (d, 2H, H-5, 5′), 7.06 (d, 2H, H-6, 6′), 2.43 (d, 2H, H-8), 1.84 (m, 1H, H-9), 0.90 (d, 6H, H-10, 10′), 0.87 (t, 9H, δ-H); 1.18-1.32 (m, 12H, H-α, β), 1.49–1.75 (m, 6H, H-γ), [^2J (^{119}Sn–^{1}H) = 55.97 Hz], [∠C–Sn–C= 109.4°][b]; ^{13}C NMR [δ (ppm), $CDCl_3$, 100.53 MHz]: 180.07 (C-1), 45.91 (C-2), 19.16 (C-3), 139.30 (C-4), 127.10 (C-5, 5′), 129.01 (C-6, 6′), 139.95 (C-7), 45.05 (C-8), 30.17 (C-9), 22.37 (C-10, 10′), 16.37 (C-α), 26.92 (C-β), 27.71 (C-γ), 13.60 (C-δ), [^1J(^{13}C–$^{117/119}$Sn) = 354.3/500.96 Hz], [∠C–Sn–C = 107.8°/120.7°].; ^{119}Sn NMR [δ (ppm), $CDCl_3$, 186.50 MHz]: 110.86.

2.4.8 | $Ph_3Sn(IBF)$, $(C_{31}H_{32}O_2Sn)$

Physical state: off-white, solid; yield: 78%, m.p.: 96 °C; MW= 556.1; Anal. calcd for $C_{31}H_{32}O_2Sn$: C 67.05, H 5.81, Sn 21.38; observed: C 66.68, H 5.34, Sn 20.91. IR (KBr, cm^{-1}): ν_{as} (C=O) 1616(s), ν_s(C=O) 1427(s), 1380(m), ν = 195 cm^{-1}, ν(C=C)/ν (ring) 1506(m), 1474(m), 1450(m), ν (Sn–O) 553(m), ν (Sn←O) 444(s); ^{1}H NMR [δ (ppm), $CDCl_3$, 399.78 MHz]: 3.83 (q, 1H, H-2), 1.50 (d, 3H, H-3), 7.19 (d, 2H, H-5, 5′), 7.04 (d, 2H, H-6, 6′), 2.44 (d, 2H, H-8), 1.84 (m, 1H, H-9), 0.90 (d, 6H, H-10, 10′), 7.65-7.63 (br, 6H, H_o); 7.42-7.37 (br, 9H, H_{mp}) [^2J($^{117/119}$Sn–^{1}H) = 51.97/59.98 Hz], [∠C–Sn–C= 108.28/112.15°][b]; ^{13}C NMR [δ (ppm), $CDCl_3$, 100.53 MHz]: 181.15 (C-1), 45.24 (C-2), 19.24 (C-3), 138.65 (C-4), 127.16 (C-5, 5′), 129.07 (C-6, 6′), 140.10 (C-7), 45.03 (C-8), 30.17 (C-9), 22.38 (C-10, 10′), 128.77, 129.07, 136.69, 138.64 ($C_{i,o,m,p}$), [^1J(^{13}C–$^{117/119}$Sn) = 390.97 Hz], [∠C–Sn–C = 111.05°][c]; ^{119}Sn NMR [δ (ppm), $CDCl_3$, 186.50 MHz]: –109.53.

2.4.9 | $\{[Me_2Sn(IBF)]_2O\}_2$, $(C_{60}H_{92}O_{10}Sn_4)$

Physical state: white, solid; yield: 78%, m.p.: 112 °C; MW= 1452.3; Anal. calcd for ($C_{60}H_{92}O_{10}Sn_4$): C 49.76, H 6.40, Sn 32.79; observed: C 49.70, H 6.02, Sn 32.16. IR

(KBr, cm^{-1}): ν_{as}(C=O) 1638, 1569(s), ν_s(C=O) 1512(s), 1459(s), ν = 231, 184 cm^{-1}, ν(C=C)/ν (ring) 1507(m), 1459(m), ν_{as} (Sn–C) /ν_s (Sn–C) 640(m), 594(m), 521(w), ν (Sn–O) 581(s), 499(s); ^{1}H NMR [δ (ppm), $CDCl_3$, 399.78 MHz]: 3.47 (q, 2H, H-2), 1.36 (d, 6H, H-3), 7.15 (d, 4H, H-5, 5′), 7.06 (d, 4H, H-6, 6′), 2.43 (d, 4H, H-8), 1.83 (m, 2H, H-9), 0.89 (d, 12H, H-10, 10′), 0.47 (6H, H-α); ^{13}C NMR [δ (ppm), $CDCl_3$, 100.53 MHz]: 180.71 (C-1), 47.00 (C-2), 18.94 (C-3), 138.97 (C-4), 127.11 (C-5, 5′), 129.25 (C-6, 6′), 140.18 (C-7), 45.02 (C-8), 30.17 (C-9), 22.34 (C-10, 10′), 5.87, 8.36 (C-α), [^1J(^{119}Sn–^{13}C) = 437.73 Hz], [∠C–Sn–C= 115.15°][c]; ^{119}Sn NMR [δ (ppm), $CDCl_3$, 186.50 MHz]: –176.78, –182.34.

2.4.10 | $Bu_2Sn(IBF)_2$ ($C_{34}H_{52}O_4Sn$)

Physical state: white, solid; yield: 89 %, m.p.: 68 °C; MW= 644.3; Anal. calcd for $C_{34}H_{52}O_4Sn$: C 63.46, H 8.07, Sn 18.45; observed: C 63.03, H 7.99, Sn 17.93. IR (KBr, cm^{-1}): ν_{as}(C=O) 1596(s), ν_s(C=O) 1389(m), ν = 206 cm^{-1}, ν(C=C)/ν (ring) 1507(s), 1464(m), ν_{as} (Sn–C) /ν_s (Sn–C) 603(m), 503(w), ν (Sn–O) 542(m), ν (Sn←O) 494(s); ^{1}H NMR [δ (ppm), $CDCl_3$, 399.78 MHz]: 3.75 (q, 2H, H-2), 1.50 (d, 6H, H-3), 7.23 (d, 4H, H-5, 5′), 7.07 (d, 4H, H-6, 6′), 2.43 (d, 4H, H-8), 1.83 (m, 2H, H-9), 0.89 (d, 12H, H-10, 10′), 0.76 (t, 6H, δ-H); 1.25-1.16 (m, 6H, H-γ), 1.42-1.56 (m, 8H, H-α, β), [^2J(^{119}Sn–^{1}H) = 71.96 Hz], [∠C–Sn–C= 121.78°][b]; ^{13}C NMR [δ (ppm), $CDCl_3$, 100.53 MHz]: 184.48 (C-1), 45.01 (C-2), 18.70 (C-3), 137.76 (C-4), 127.14 (C-5, 5′), 129.15 (C-6, 6′), 140.49 (C-7), 45.01 (C-8), 30.15 (C-9), 22.35 (C-10, 10′), 24.84 (C-α), 26.41 (C-β), 26.08 (C-γ), 13.42 (C-δ): ^{119}Sn NMR [δ (ppm), $CDCl_3$, 186.50 MHz]: –146.07.

s, Singlet; d, doublet; t, triplet; m, multiplet; br, broad; dd, doublet of doublet; q, quartet; [b]determined through Lockhart Manders equation 27; [c]determined through Lockhart Manders equation 28; m, medium; s, strong; w, weak, br, broad for IR frequencies.

3 | RESULTS AND DISCUSSION

3.1 | Chemistry

Triorganotin(IV) complexes of IBF (**1–3**) were synthesized by refluxing Me_3SnCl/Bu_3SnCl/Ph_3SnCl with sodium salt of IBF (1:1 metal to ligand ratio) in methanol with a continuous supply of dry nitrogen as given in Scheme 1(a). NaCl formed during the reaction was removed by washing the complexes with a mixture of MeOH and H_2O (9:1, v/v). Complex **4** was prepared by refluxing Me_2SnCl_2 and IBF with equivalent NaOH, Scheme 1(b), so as to form IBF–dimethyltin hydroxide intermediate which then further refluxed in the presence of Na_2SO_4 in order to absorb H_2O formed during the course of reaction, which is necessary for the reaction to complete. Further, complex **5** was synthesized by microwave irradiation of a mixture of Bu_2SnO and IBF in 1:2 (metal to ligand) ratio [Scheme 1 (c)]. The reaction proceeded, as the water molecules formed during the course of reaction evaporated with microwave irradiation. The whole reaction was completed in 5 min and yield was quite high. All of the complexes prepared were soluble in methanol, $CHCl_3$ and acetonitrile, and stable towards air and moisture. The melting point, physical and analytical data of complexes are given in the Experimental section. The CHSn percentages observed for the proposed structure of the complexes was very close to the calculated values. The proposed structures and synthetic route opted for the synthesis of complexes **1–5** are given in Scheme 1. The structures of the complexes **6–19** as reported previously[20–22] are given in Scheme 2.

3.1.1 | X-ray crystallography of complex 3 [$Ph_3Sn(IBF)$]

The relevant crystallographic data and the structure refinement parameters are organized in Table 1, and the selected bond lengths, bond angles and torsions angles are systematically compiled in Table 2. An ORTEP view of the complex **3** is illustrated in Fig. 1. The X-ray diffraction examination apparently reveals that the complex seems to crystallize in a monoclinic space group 'P 21/n' and comprises four molecules associated with weak van der Waal's C–H...π interactions (2.883 Å) among the phenyl groups at Sn atoms in its unit cell. The complex may be perceived to adopt a distorted capped tetrahedral (Td) geometry (interpreted as a [4+1] coordinated geometry around the Sn atom) wherein the O atoms of the carboxylate group are bonded in an asymmetric chelating mode to the Sn atom through a weak and a strong bonds as evident from the values of the observed Sn–O and O–C bonds lengths, *viz.* Sn(1)–O(1) 2.633 Å, Sn(1)–O(2) 2.079 Å, O(1)–C(19)1.224 Å and O(2)–C(19) 1.301 Å. The strong covalent bond [Sn(1)–O(2) 2.079 Å] was found to be consistent with the earlier reports on similar triorganotin(IV) carboxylates wherein the Sn–O bonds were measured to be 2.077 and 2.0748 Å, respectively.[29,30] On the contrary, the weak bond [Sn(1)–O(1) 2.633 Å] is much shorter than the van der Waal's radii of the respective atoms (3.7 Å), and therefore, it is considered as a weak coordinate (Sn←O) bond, which is akin to the earlier measured value (2.671Å) for the similar triphenyltin(IV) complex.[30] It is obvious that on account of the weak Sn←O bond, the structure of complex **3** underwent a significant distortion from ideal Td to TBP geometry and can best be described

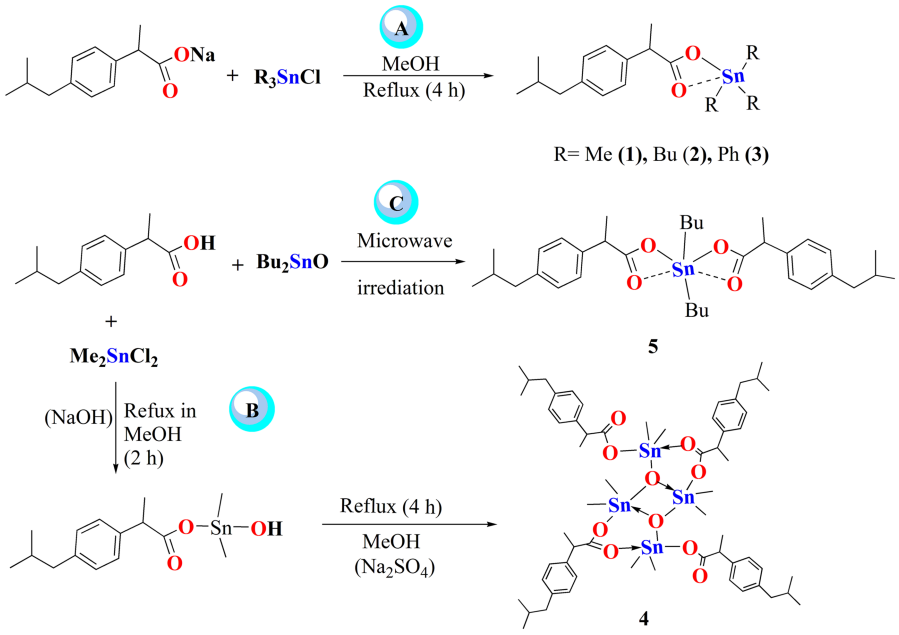

SCHEME 1 Synthetic routes for complexes **1–5.**

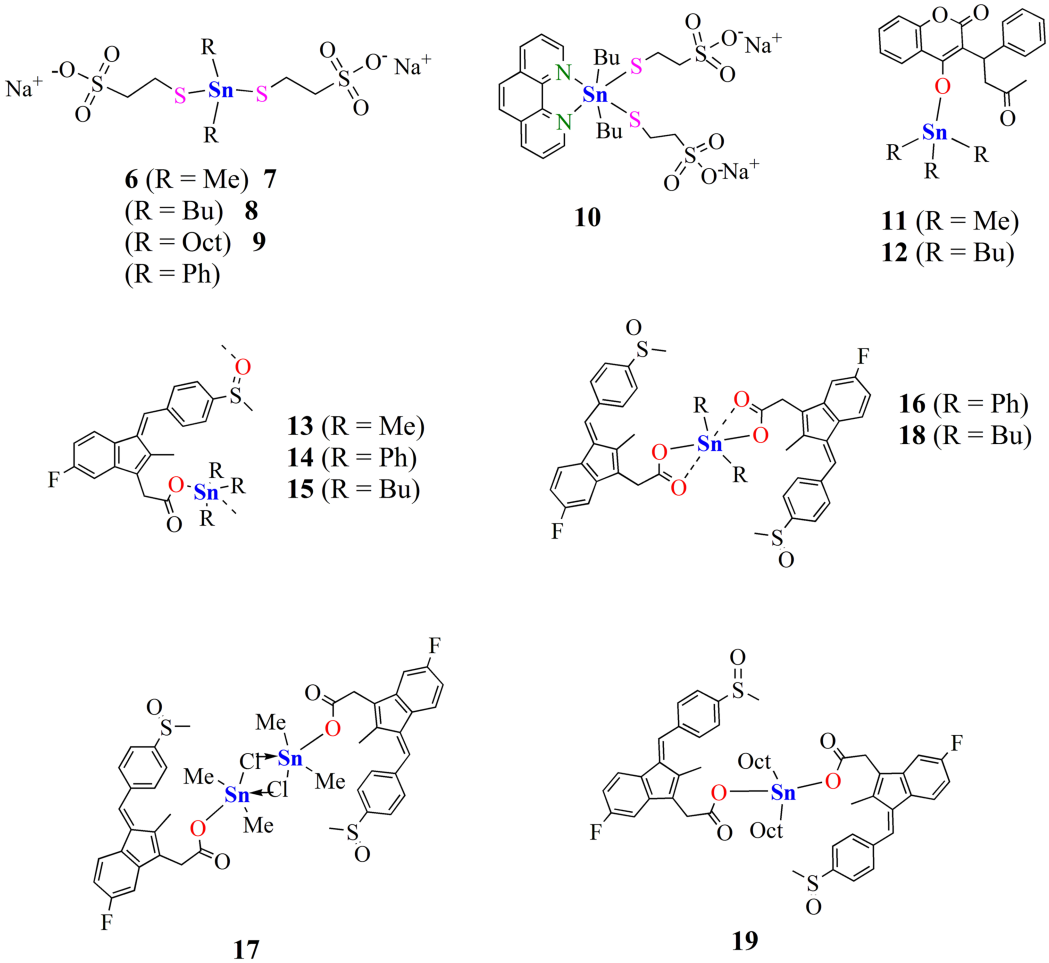

SCHEME 2 Structures of organotin(IV) complexes of different drugs: **6** [$Me_2Sn(MESNA)_2$], **7** [$Bu_2Sn(MESNA)_2$], **8** [$Oct_2Sn(MESNA)_2$], **9** [$Ph_2Sn(MESNA)_2$], **10** [$Bu_2Sn(MESNA)_2$·Phen], **11** {[$Me_3Sn(WR)$]}, **12** [$Bu_3Sn(WR)$], **13** [$Me_3Sn(Sul)$], **14** [$Ph_3Sn(Sul)$], **15** [$Bu_3Sn(Sul)$], **16** [$Ph_2Sn(Sul)_2$], **17** [$Me_2SnCl(Sul)]_2$, **18** [$Bu_2Sn(Sul)_2$] and (**19**) [$Oct_2Sn(Sul)_2$]. MESNA, Sodium 2-mercaptoethanesulfonate; warfarin (WR), 2H-1-benzopyran -2-one-4-hydroxy-3-(3-oxo-1-phenylbutyl); sulindac (SUL), 2-{5-fluoro-1-[(4-methanesulfinylphenyl)methylidene]-2-methyl-1H-inden-3-yl}acetic acid.20–22

TABLE 1 Crystallographic data and structure refinement parameters for [Ph_3Sn(IBF)].

	[Ph_3Sn(IBF)]
Empirical formula	$C_{31}H_{32}O_2Sn$
Formula weight	555.26
Crystal system	Monoclinic
Space group	*P* $2_1/n$
a (Å)	11.423(5)
b (Å)	9.318(5)
c (Å)	26.005(5)
β (deg)	97.298(5)
V (Å^3)	2746(2)
Z	4
$D_{calc.}$ (g cm^{-3})	1.382
μ (mm^{-1})	0.954
T (K)	293 (2)
F000	1136
λ (Mo k*α*) (Å)	0.71073
θ_{min} (deg)	2.46
θ_{max} (deg)	29.64
Total reflections	31500
Reflections collected	5777
Data/restraints/parameters	6840/1/307
wR_2 (all data)	0.1006
wR_2	0.0952
R_1 (all data)	0.0512
R_1	0.0408
Largest difference peak	0.769
Deepest hole	−0.932
Goodness-of-fit	1.095

TABLE 2 Selected bond lengths (Å), bond angles (deg) and torsion angles (deg) with estimated standard deviations for [Ph_3Sn(IBF)].

Bond lengths			
Sn(1)–O(1)	2.633(2)	O(1)–C(19)	1.224(4)
Sn(1)–O(2)	2.079(2)	O(2)–C(19)	1.301(4)
Sn(1)–C(1)	2.137(3)	C(1)–C(2)	1.361(5)
Sn(1)–C(7)	2.136(3)	C(20)–C(21)	1.518(5)
Sn(1)–C(13)	2.133(3)	C(22)-C(23)	1.380(5)
Bond angles			
O(1)–Sn(1)–O (2)	53.88(9)	O(2)–Sn(1)–C(13)	104.11(10)
O(1)–Sn(1)–C (1)	85.2(1)	C(1)–Sn(1)–C(7)	107.97(12)
O(1)–Sn(1)–C (7)	148.0(1)	C(1)–Sn(1)–C(13)	119.31(12)
O(1)–Sn(1)–C (13)	83.6(1)	C(7)–Sn(1)–C(13)	112.45(13)
O(2)–Sn(1)–C (1)	115.82(10)	Sn(1)–O(1)–C(19)	80.6(2)
O(2)–Sn(1)–C (7)	94.54(11)	Sn(1)–O(2)–C(19)	104.7(2)
Torsion angles			
O(1)–Sn(1)–O (2)–C(19)	3.5(2)	O(1)–Sn(1)–C(1)–C(6)	157.5(3)
O(2)–Sn(1)–C (1)–C(6)	111.8(3)	C(1)–Sn(1)–O(1)– C(19)	-130.8(2)
C(1)–Sn(1)–O (2)–C(19)	65.5(2)		

Symmetry operations: (i) *x*, *y*, *z*; (ii) −*x*+1/2, *y*+1/2, −*z*+1/2; (iii) −*x*, −*y*, −*z*; (iv) *x*−1/2, −*y*−1/2, *z*−1/2.

as a capped tetrahedron.[29,30] In addition to the values of the measured bond angles, *viz.* C–Sn–C (107.97–119.31°), O–Sn–C (83.6–148.0°) and O–Sn–O (53.88°), and the torsions angles, *viz.* O(1)–Sn(1)–O(2)–C(19) 3.5°, O(1)–Sn(1)–C(1)–C(6) 157.5°, O(2)–Sn(1)–C(1)–C(6) 111.8°, C(1)–Sn(1)–O(1)–C(19) −130.8° and C(1)–Sn(1)–O(2)–C(19) 65.5°, further substantially support the severe distortion, which seems to be considerably deviated from their ideal values. Further, the stability of crystal lattice can be described by weak van der Waal's forces among the phenyl groups of the adjacent molecules.

3.1.2 | FTIR spectroscopy

A broad band in the region 2500–3300 cm^{-1} represents the stretching frequency of the O–H group of carboxylic acid. Its disappearance after complexation to Sn atom reveals the deprotonation of carboxylate oxygen. Weakening of the C=O bond after complexation can be explained with a shift in *ν*(C=O) towards lower frequencies. The diagnostic bands for the carboxylate antisymmetric [ν_{as} (OCO)] and symmetric [ν_s (OCO)] stretching vibrations of complexes **1–5** appeared in the range 1569–1638 and 1356–1427 cm^{-1}, respectively, which could have not been assigned without the formation of complexes.[31–34] A measure of difference of ν_{as} (OCO) and ν_s (OCO) (*ν*) is important to estimate the probable mode of binding of carboxylates to Sn metal. The complexes **1–3** and **5** show *ν* values 186–206 cm^{-1} which are comparable with the sodium salt of the ligand (IBF) and reveals a bidentate mode of coordination of carboxylate group with the metal. However, two different *ν* values, 231 and 184 cm^{-1}, were observed for complex **4**, which revealed the occurrence of two different modes of binding of carboxylate.[35] Strong-

to medium-intensity bands appeared in the region 581–444 cm^{-1} and were assigned to Sn–O and Sn←O stretching frequency, which clearly indicated the formation of complexes. Furthermore, the characteristic bands found in the regions 635–597 and 597–503 cm^{-1} could be assigned to ν_{as} (Sn–C) and ν_s (Sn–C) modes, respectively, in di- and trialkyltin derivatives.[31,36] In addition, a sharp band with strong intensity was detected at 635 cm^{-1} which could be assigned to the ν (Sn–O–Sn) mode in complex **4.**[32,36] Data pertaining to the FTIR studies of complexes, the drug and its sodium salt are presented in the Experimental section. FTIR spectra of all complexes are given in the Supporting Information as Figs S1–S3.

3.1.3 | Multinuclear (^{1}H, ^{13}C and ^{119}Sn) NMR spectroscopic studies

Characterization and structural determination of synthesized complexes was performed by multinuclear NMR studies and ^{1}H, ^{13}C and ^{119}Sn NMR data for the synthesized complexes are given in the Experimental section. ^{1}H NMR data revealed the correct integration of protons as expected according to the plausible structures of complexes **1–5.** A relevant shift was observed in the ^{1}H chemical shifts of IBF after complexation which evidenced the formation of complexes**.** The heteronuclear one-bond (^1J) and two-bond coupling (^2J) constants play a significant role in determining the ∠C–Sn–C, thus predicting the geometry of the complexes. The values of $^2J(^{119}Sn–^1H)$ obtained for **1–3** were 57.60, 55.97 and 51.97/59.98 Hz, respectively, and those of ∠C–Sn–C calculated from Lockhart and Mander's equation[27,28] were 110.8°, 109.4° and 108.28/112.15°, respectively, which are in the range of four-coordinated tin atom and revealed tetrahedral geometries for these complexes in solution state.[28,29] These results are in contrast with the pseudo five or 4+1 type of coordination of Sn atom, revealed on the basis of crystal structure of complex **3** and similar geometry proposed for complexes **1** and **2** in solid state. This can be explained by the dissociation of the weak coordinate bond between tin and carbonyl oxygen of the drug molecule in solution state. The resolved $^2J(^{119}Sn–^1H)$ value for complex **5** was 71.96 Hz and the calculated ∠C–Sn–C was 121.78°, which lie in the range of the octahedral coordinated Sn atom.[28] Since the FTIR data of complex **5** revealed a similar kind of bidentate mode of coordination for both the carboxylate groups attached to Sn, the Sn atom should be hexa-coordinated. No satellite peaks were resolved for complex **4**, hence $^2J(^{119}Sn–^1H)$ and ∠C–Sn–C could not be calculated. ^{13}C NMR spectra of complexes revealed a downfield shift in resonance of carboxylate carbon compared with the free ligand owing to the drift of electron density towards tin metal. C2 and C3 carbon also showed significant downfield shift for similar reasons. One-bond coupling constant $[^1J(^{119}Sn–^{13}C)]$ values for complexes **1** and **3** were 388 and 390.97 Hz and calculated values of ∠C–Sn–C were 110.8° and 111.05°, respectively, which are similar to those calculated from the $^2J(^{119}Sn–^1H)$ value. The coupling constant $[^1J(^{119}Sn–^{13}C)]$ and ∠C–Sn–C value for complex **4** were 437.73 Hz and 115.15°, respectively, which describe a penta-coordinated geometry around tin metal. Two different resonances observed in ^{13}C NMR spectra of methyl carbon (attached to tin) explained the two different tin environments in complex **4.**[21] A single resonance observed for carboxylate carbon of this complex could be due to either accidental magnetic equivalence or dynamic equilibrium between different isomeric structures.[21] ^{119}Sn NMR resonances for **1–3** (136.16 ppm, 110.86 ppm and –109.53 ppm) further support the tetrahedral geometry for these complexes. However, two values of ^{119}Sn resonances at –176.78 and –182.34 ppm for complex **4** suggested a penta-coordinated geometry around tin atoms with two different environments.[21,37–39] which can be justified by the tetra-nuclear tin structure as given in Scheme 1 (c). For complex **5**, the ^{119}Sn NMR chemical shift value is –146.07, which is similar to the other complexes reported in the literature[37,39,40] for a highly distorted octahedron or bicapped tetrahedron type of geometry. ^{1}H, ^{13}C and ^{119}Sn NMR spectra of complexes are presented in the Supporting Information as Figs S4–S12.

3.1.4 | ESI–MS spectrometry

The ESI–MS spectrometric data for synthesized complexes were recorded in the range m/z 200–1500, using acetonitrile solvent (HPLC grade) in positive-ion mode. All of the complexes were characterized by molecular ion peaks corresponding to m/z, $[M+Na]^+$ and $[M+K]^+$, where the m/z ratio owing to $[M+Na]^+$ is always a base peak. The isotopic patterns (m/z) owing to associated molecules/organotin moieties and fragmented ions found for few complexes are listed in Table S1 (ESI file). The fragmentation pattern of complex **4** is illustrated in Scheme S1. HRMS spectra of complexes **1–5** are given in Figs S13–S15.

3.1.5 | Geometry optimization through DFT calculations

Structures of the complexes were designed with the help of Chemcraft software and then subjected to full geometry optimization in the gaseous phase through Gaussian 09 software package.[41] The drug molecule (IBF) and complexes **1–5** were optimized with B3LYP function, and 6–31G (d,p) and LANL2DZ basis set, respectively. All of the

imaginary frequencies in the harmonic frequency calculation are zero, which implies that the optimized geometries are very likely at global minima on the potential energy surface. Figure S16 presents the optimized structure of IBF and complexes **1–5**. Triorganotin derivatives of IBF, i.e. complexes **1–3** were optimized as distorted tetrahedral geometries, owing to weak interaction between the carbonylic oxygen with Sn atoms. The C–Sn–C angles obtained from the optimized geometries were in good agreement with the corresponding calculated angles and are presented in Table S2. Further, good agreement between the selected bond lengths and bond angles observed from the crystal structure of complex **3** and its optimized geometry was found. Compound **4** exhibited a dimer distannoxane, in which the planar Sn_2O_2 core was linked to two exo-cyclic Sn moieties through the bridged oxygen atoms. The coordination geometry for the endo Sn atom was a distorted square pyramidal type with O atom of Sn_2O_2 core at the top of the pyramid and two methyl groups *trans* to each other. However, the exo Sn atom had a distorted trigonal bipyramidal geometry having methyl groups *cis* to each other and axial positions occupied with O atoms of two carboxylate groups as illustrated in Fig. S16. The bond angle and bond lengths observed were in good approximation with similar reported complexes.[36–38] Complex **5** was optimized as a highly distorted octahedral geometry, sometimes considered as bicapped tetrahedron with two carboxylate oxygen capping the faces. Herein, the carboxylate groups were said to be coordinated in an anisobidentate fashion, with covalent and coordinate Sn–O bonds 2.027 and 2.99 Å, respectively, which were significantly shorter than van der Waal's radii.[37,38,40] Frequencies calculated through DFT for IBF and complexes **1–5** were found to be in good correlation with that experimentally obtained for corresponding compounds. Table S2 provides the important outcomes of the DFT calculation. Frontier molecular orbitals (HOMO–LUMO) generated by Gaussian 09 are given in Fig. S17. In free ligands HOMO and LUMO are distributed over the carboxylic acid group and phenyl ring of IBF; however, with the formation of complexes HOMO remains on the IBF part and LUMO is shifted towards the tin metal.

3.2 | Biological studies

3.2.1 | DNA binding studies

UV–vis spectrophotometric studies

Ibuprofen and organotin complexes show UV–vis bands with absorption maxima (λ_{max}) around 222, 264 and 273 nm owing to π–π^* and n–π^* electronic transitions. The bands around $\lambda_{max,}$ 222 and 264 nm, were chosen as the specific wavelengths for the CT DNA interaction study, because a significant amount of change was associated with them with successive addition of CT DNA. A careful observation of changes in absorbance owing to IBF/complexes is insightful to estimate their mode of interaction with DNA. For IBF, a hyperchromic effect in UV bands for the first few addition of DNA (until 6 μM)

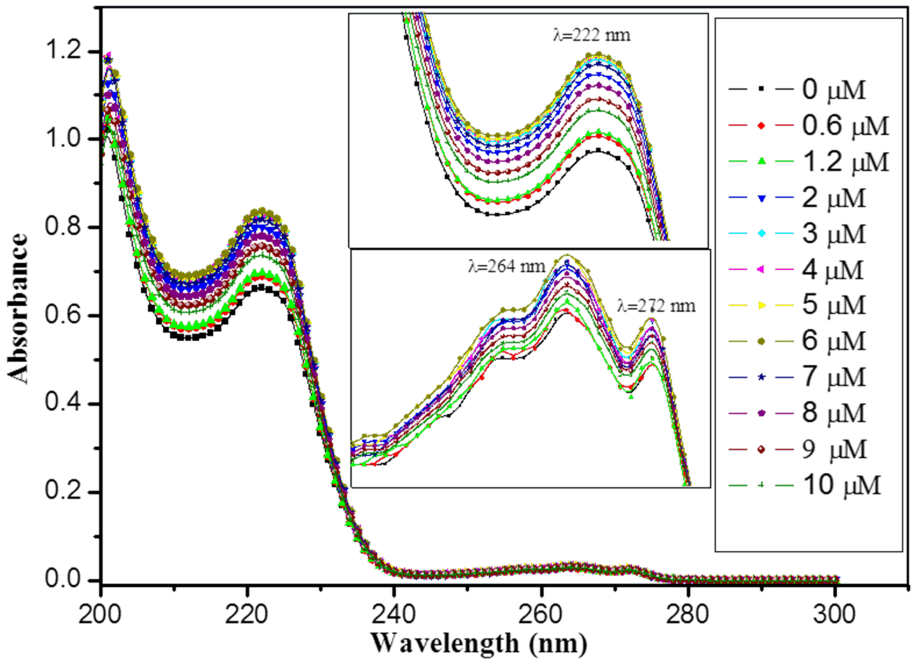

FIGURE 2 UV–vis spectra of IBF [6.7×10^{-5} M] (a), in the absence and presence of CT DNA [0.6–15 μM] in Tris–HCl/NaCl (5:50 mM) buffer, pH 7.2 at 25 °C. (i, ii) Expanded region of UV bands at $\lambda_{max,}$ 222 and 264 nm, respectively

was observed, which was followed by a continuous decrease in absorbance shown in Fig. 2(a). Similarly, a sudden hyperchromicity followed by a gradual hypochromic effect [Fig. 3(d)] was involved in the case of the dibutyltin(IV) derivative of IBF i.e. complex **5**. These changes suggested the involvement of different modes of binding in the case of IBF and complex **5.** For complex **1** [Me_3Sn(IBF)] a significant hyperchromic effect at both bands was observed, whereas complex **2** [Bu_3Sn(IBF)] showed a significant increase in the absorbance at λ_{max} 222 and a slight decrease in absorbance at band 263 nm with successive addition of CT DNA. This significant hyperchromism centred at the λ_{max} 222 nm in complexes **1** and **2** [Fig. 3(b) and (c)] is suggestive of a strong interaction of complexes with DNA and the spectral changes indicate the possibility of groove binding or electrostatic interactions.[19,42,43] These studies alone are not very insightful for determining the mode of interaction of IBF/complexes with CT DNA, which has been further discussed through fluorescence experiments.

Fluorescence titration studies

The interactions of IBF and complexes with CT DNA were further investigated through fluorescence titra-

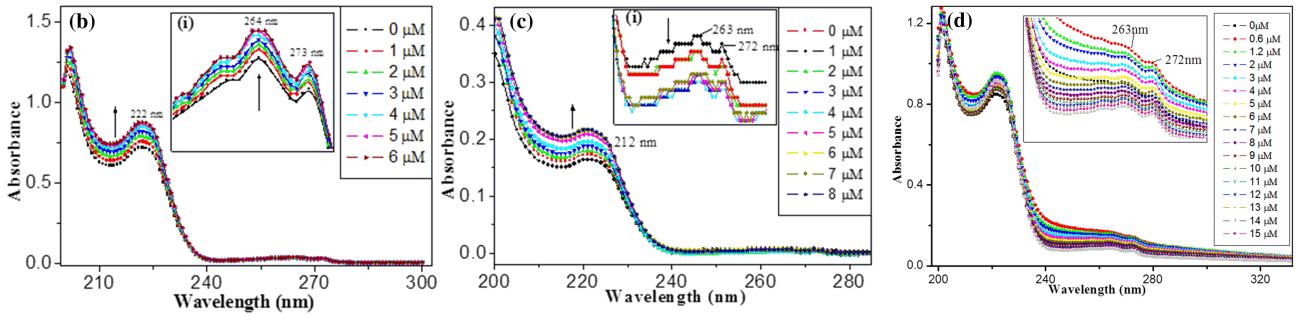

FIGURE 3 UV–vis spectra of complexes [6.7×10^{-5} M]: (b) complex **1**; (c) complex **2**; and (d) complex **5**, in the absence and presence of CT DNA [0.6–15 μM] in Tris–HCl/NaCl (5:50 mM), buffer, pH 7.2 at 25 °C. (i, ii) Expanded region of UV bands at $\lambda_{max,}$ 221/222 and 263/264 nm, respectively. The arrows indicate the increase/decrease in absorbance with increasing DNA concentration

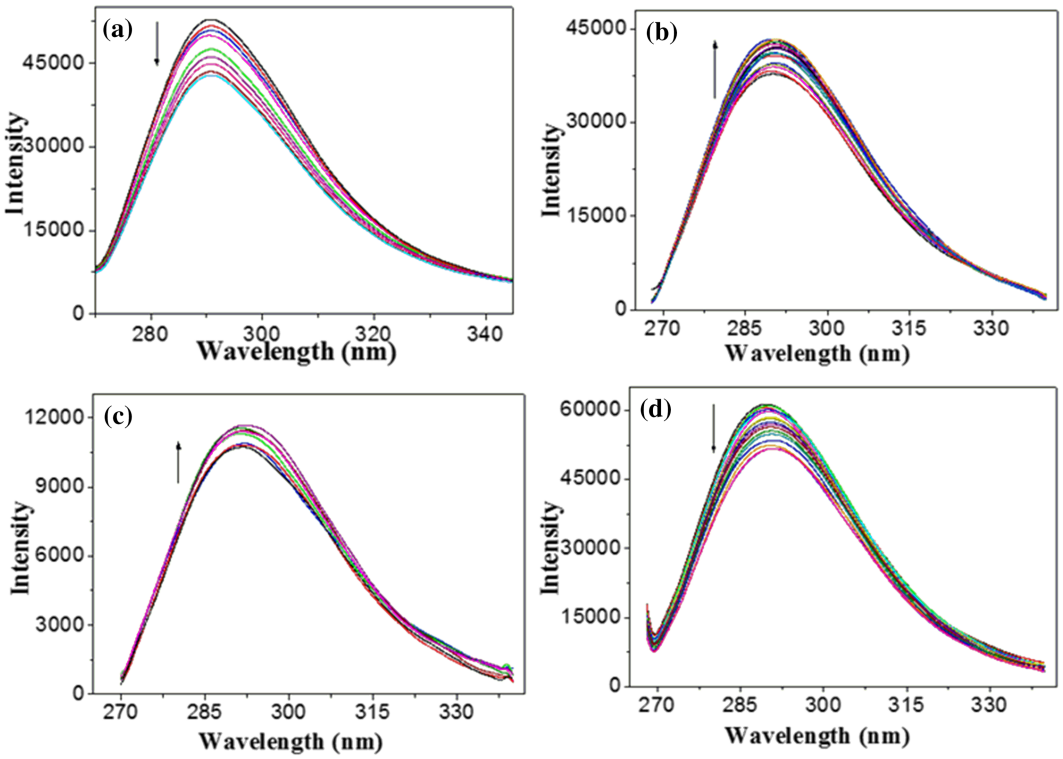

FIGURE 4 Emission spectra of IBF (66.7 μM) (a) and complexes (66.7 μM) **1** (b), **2** (c) and **5** (d) in the absence and presence of CT DNA (2–20 μM) in Tris–HCl/NaCl (5:50 mM) buffer, pH 7.2 at 25 °C. Arrows indicate the increase/decrease in emission intensity with increasing concentration of DNA

tions. Complexes **1**, **2** and **5** were found to exhibit strong emission in the range 270–360 nm (emission maxima around 290 nm). The significant decrease in fluorescence intensity of IBF and complex **5** along with a small red shift (2–3 nm) (Fig. 4) with successive addition of CT DNA (2–20 μM) indicates an intercalation of these molecules within the base pairs of DNA. The intercalation of molecules within the DNA base pairs restricts their rotational motion, which favours the deactivation of the excited states through radiationless processes,[8] which are generally associated with quenching of the fluorescence intensity as in the case of IBF and complex **5**. The increase in fluorescence intensity with minimal red shift (1–2 nm) was observed for complexes **1** and **2**, which indicates the possibility of the groove binding or electrostatic interactions. Further, the partial intercalative mode of binding could not be ruled out for these complexes.

EB quenching assay

Being a planar aromatic compound, EB intercalates strongly within the base pairs of DNA. EB shows weak emission spectra in the aqueous solution; however, its emission intensity increases many fold after intercalation within the hydrophobic environment of DNA. This is because of shielding of EB molecules from the polar solvent, which reduces its quenching.[7] In order to obtain insight into the binding mode of IBF and complexes with CT DNA, an EB displacement experiment was performed. The results of the experiment (Fig. 5) reveal a continuous decrease in emission intensity of the EB–DNA adduct with subsequent addition of IBF and complexes **1**, **2** and **5**, which suggests that the molecules are able to displace the EB from the intercalated sites of DNA and set it free in the solvent, which leads to a decrease in its emission intensity. The quenching constants (K_{sv}) (given in Table S3) are on the order of 10^3–10^4 for IBF and complexes. The results reveal that IBF and complex **5** compete strongly with EB for the available intercalation sites in DNA compared with complexes **1** and **2**. The above findings suggest that IBF and complex **5** bind with DNA through moderate intercalation.[32,43] However, a lesser decrease in emission intensity of the EB–DNA adduct with the addition of complexes **1** and **2** indicates that the complexes may bind through either non-intercalative (groove binding or electrostatic interaction) or a partial interacalative mode of interaction.

Fluorescence studies in the presence of KI

KI is an anionic quencher, which can quench the emission intensity of small molecules. However, it cannot quench the emission of molecules which intercalate within the DNA base pairs, because of the repulsion

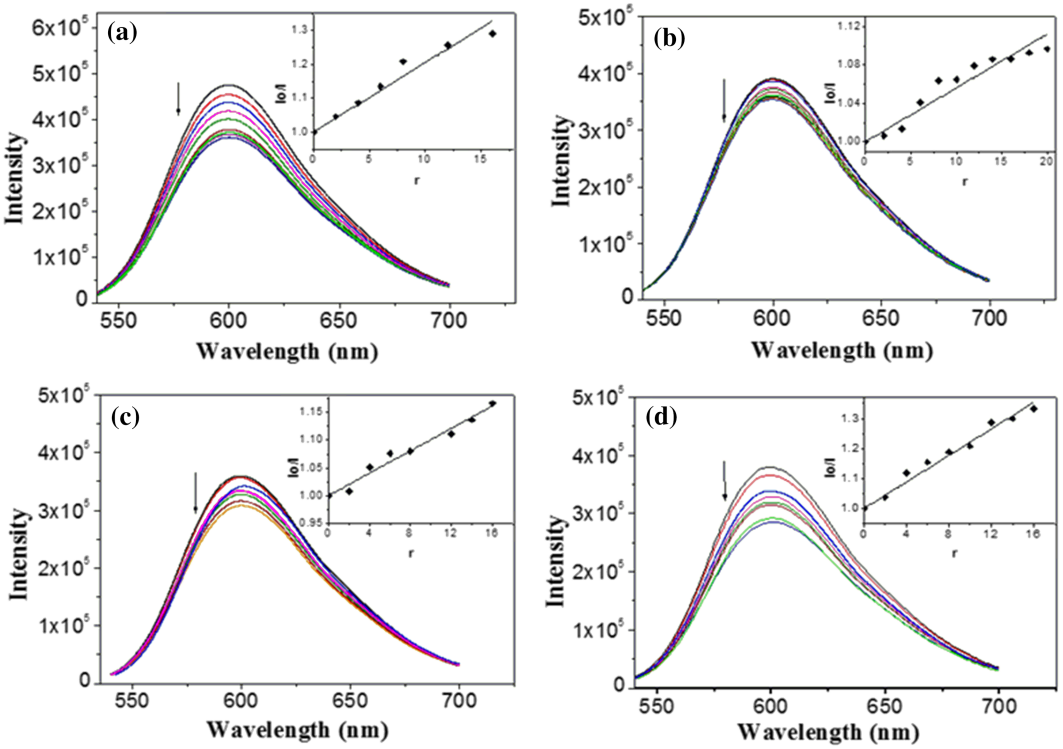

FIGURE 5 Fluorescence quenching titration spectra of EB–CT DNA ([DNA]/[EB] = 4) with successive addition of (2 – 20 μM) IBF (a), **1** (b). **2** (c) and **5** (d), in Tris–HCl/NaCl (5:50 mM) buffer, pH 7.2 at 25 °C (excitation λ_{max} at 515 nm). Inset shows linear Stern–Volmer plots and arrow indicates a decrease in intensity with increasing concentration of quenchers

experienced by negatively charged phosphate group of nucleotides.[44] However, the groove binders or electrostatic binders can be easily disturbed by the quencher.[45,46] The present study reveals a significant reduction in fluorescence intensity of IBF and complex **5** in the presence of DNA compared with that in the absence of DNA, which indicates the intercalation of these molecules inside the DNA, which protects them from being quenched. Complexes **1** and **2** show a very insignificant change in emission intensity in the presence and absence of DNA as revealed by Fig. 6. The listed K_{sv} values calculated by the Stern–Volmer equation (given in Table S4) suggest a non-intercalative type of interaction for complexes **1** and **2**. These results corroborate our previous findings as described in Section .

Viscosity measurements

The viscosity of CT DNA is regarded as quite sensitive towards any structural change in DNA, hence viscosity measurement of DNA with different concentrations of compounds in solution gives a lucid picture of their binding model with DNA. The classical intercalation of the molecule in DNA lengthens the helix of DNA. In order to accommodate the bound ligand, separation of base pairs occurs which leads to an increase in viscosity of DNA. However, partial or non-classical intercalators could cause bending or kinking in the DNA helix, which results in a reduction of its length and concomitantly its viscosity.[47] Furthermore, the non-intercalators (electrostatic and groove binder) cause a less significant change in viscosity of DNA.[7] Figure 7 illustrates a change in the specific viscosity (η) with different concentration ratios of the complex to CT DNA. A remarkable increase in DNA viscosity with increasing concentration of IBF and complex **5** reveals an intercalative mode of binding of them with DNA. A groove binding or external interactions with DNA was suggested for complexes **1** and **2** as they caused very little change in the viscosity of DNA.

All the bio-physical experimental observations evidenced the occurrence of different modes of binding for different complexes with CT DNA. An intercalative mode of binding of IBF with DNA was suggested, which is in accordance with the literature report.[8] Complex **5** also interacts with DNA through intercalative mode, but slightly more than IBF, as evidenced from the K_{sv} value in the EB displacement experiment and the fluorescence experiment with KI. A slight increase in the binding propensity can be explained on the basis of the presence of dibutyltin moieties in complex **5**, which may facilitate the intercalation of IBF inside the base pairs by providing additional hydrophobic interaction with DNA. A groove binding or external binding of complexes **1** and **2** with DNA was revealed from UV–vis, fluorescence and viscosity measurements.

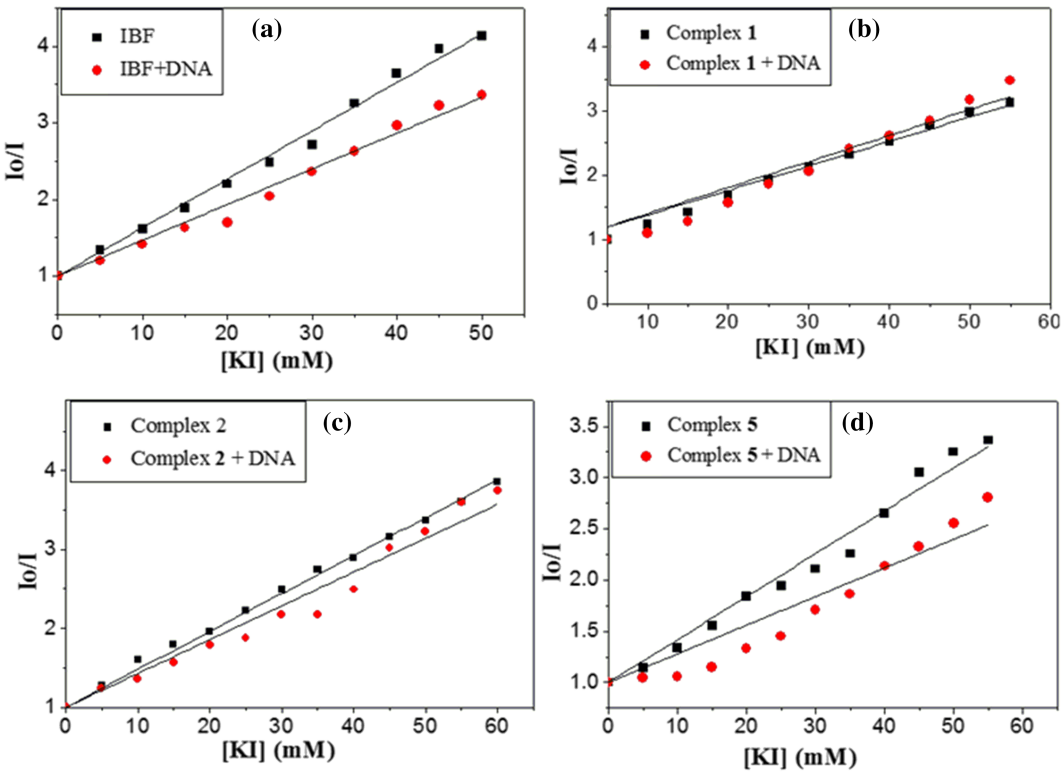

FIGURE 6 Stern–Volmer plots obtained from fluorescence quenching of IBF (66.7 μM) (a) and complexes (66.7 μM) **1** (b), **2** (c) and **5** (d) by KI (0–72 mM), in the presence and absence of CT DNA (20 μM) in Tris–HCl/NaCl (5:50 mM) buffer, pH 7.2 at 25 °C

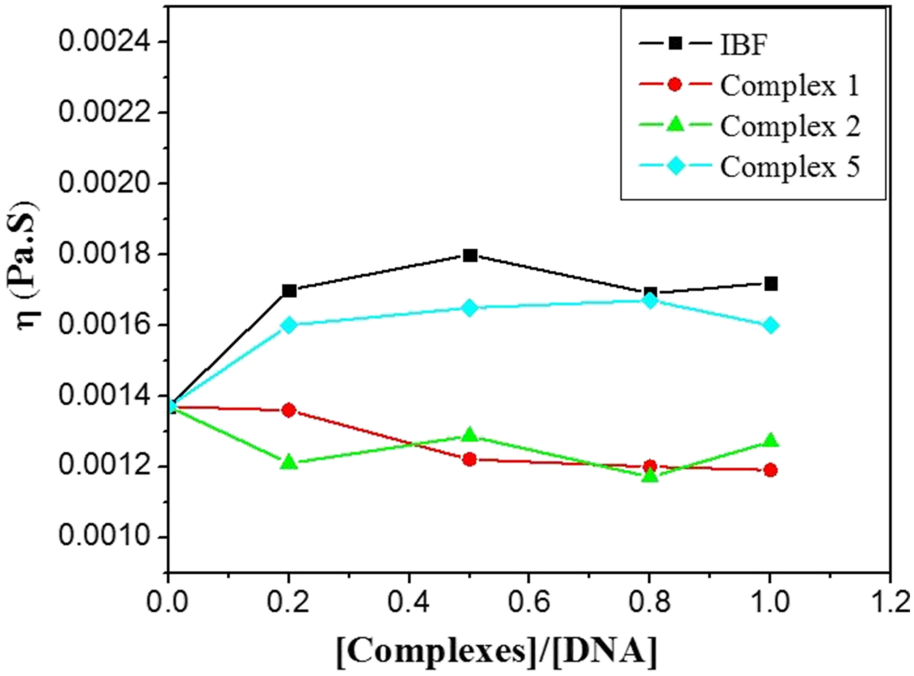

FIGURE 7 Change in viscosity (η) of CT DNA (100 μM) with successive addition of IBF and complexes **1**, **2** and **5** (0–100 μM), in Tris–HCl/NaCl (5:50 mM) buffer, pH 7.2 at 25 °C

3.2.2 | Plasmid DNA cleavage activities

DNA cleavage activities with organotin complexes have been extensively studied because of their potential to cleave supercoiled (SC) pBR322 DNA. One-strand cleavage of circular SC DNA results in a slow-moving nicked circular (NC) form, and cleavage of both strands produces a linear (L) form, which positioned itself between nicked and supercoiled forms[48,49] as the DNA moves under the influence of electric field. The cleavage pattern of plasmid DNA owing to IBF and complexes **1**, **2** and **5** was analysed with their increasing concentrations (20, 40, 60 and 80 μM) in successive lanes and in the presence of activator (ascorbic acid). Bands *viz.* Form I (SC), Form II (NC) and Form III (L) formed by the cleavage of plasmid DNA and the corresponding normalized area occupied by the different forms are presented in Fig. 8, which clearly illustrate a continuous increase in cleavage activity with increasing concentration of IBF and complexes in lanes I–IV. A gradual decrease in SC form (Form I) associated with moderate increase in NC form (Form II) and (Form III) revealed a significant cleavage activity of IBF and complexes. Moreover, the presence of H_2O_2 (lane VI), which is a hydroxy radical generator and acts as an activator in the DNA cleavage activity, enhances the cleavage activity significantly in all cases. The maximum cleavage activity was observed for the dibutyltin derivative of IBF (complex **5**), which shows the importance of organotin moiety in the process of DNA cleavage. Further, to explore the underlying mechanism of cleavage activity by the compounds under study, the cleavage experiment was run in the presence of a singlet oxygen quencher NaN_3 (lane VII) and hydroxy radical scavenger, DMSO (lane VIII). In the presence of DMSO a partial inhibition in the cleavage of pBR322 DNA was observed for IBF and complexes **2** and **5**, as shown by a decrease in NC and L band intensities in lane VIII compared with lane V (having the same IBF/complex concentrations), as clearly illustrated in Fig. 8. These findings suggest the involvement of hydroxyl radical in the DNA cleavage process. However, little difference was observed for complex **1** in the presence of DMSO, but a small decrease in NC form in the presence of NaN_3 could not be denied, which suggests the possibility of DNA cleavage through the involvement of reactive oxygen species for complex **1**. However, for IBF and complexes **2** and **5** such inhibition was not seen, which rules out the involvement of singlet oxygen.

3.2.3 | Anticancer activities

Cytotoxicity study (MTT assay)

The *in vitro* MTT assay using human cell lines provides important information about compound cytotoxicity. The mentioned drug molecules and their organotin(IV) complexes **1–19** were screened *in vitro* for cytotoxicity against selected panels of human cancer cell lines on

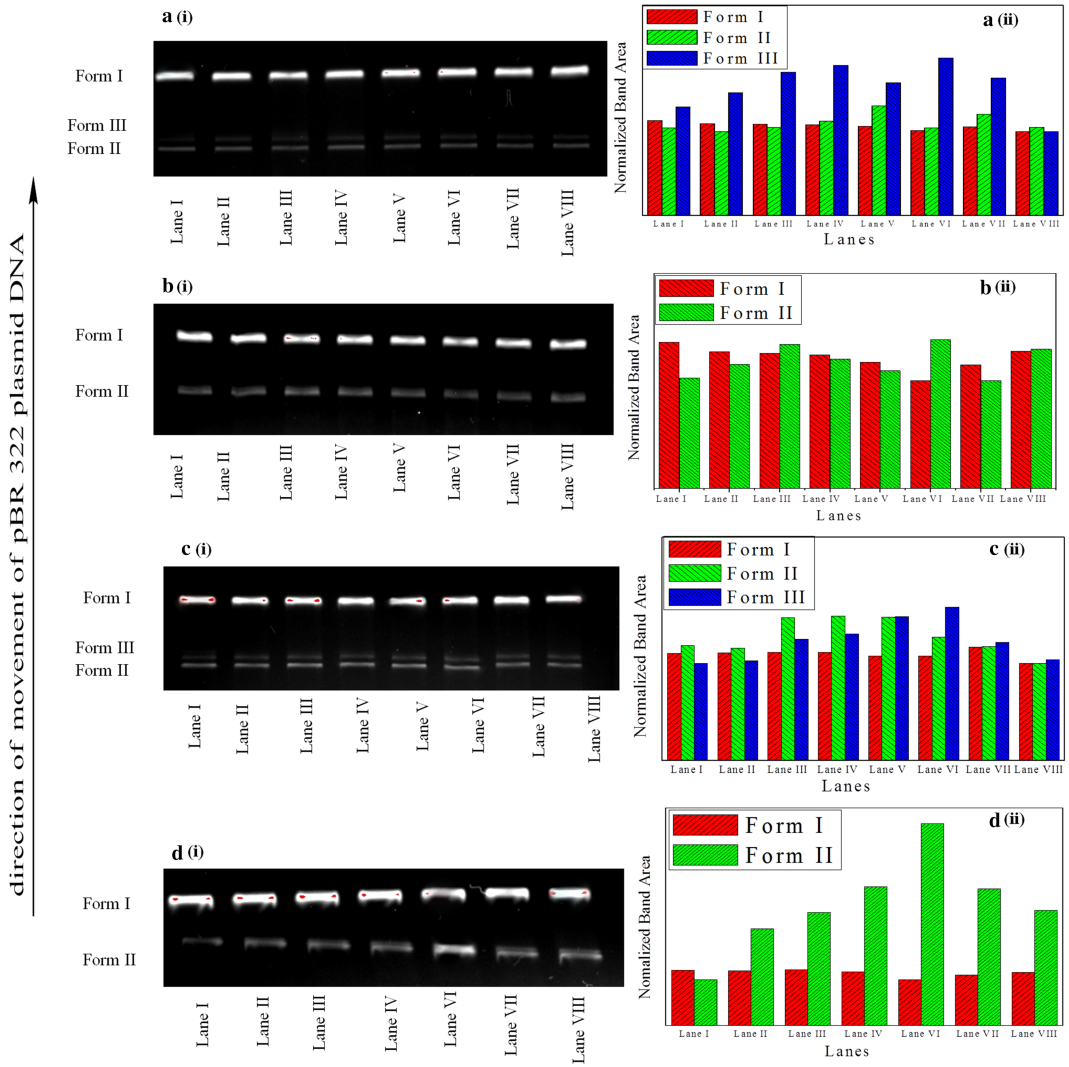

FIGURE 8 The cleavage pattern of pBR322 plasmid DNA (100 ng) by IBF (a), complex **1** (b), complex **2** (c) and complex **5** (d), after incubation for 5 h at 37 °C, at different concentrations of IBF/complexes, in Tris–HCl/NaCl (5:50 mM), buffer, pH 7.2 at 25 °C. Lane I, Control (DNA); lane II, [DNA + (20 μM complex/IBF)]; lane III, [DNA + (40 μM complex/IBF)]; lane IV, [DNA + (60 μM complex/IBF)]; lane V, [DNA + (80 μM complex/IBF)]; lane VI, [DNA + (0.2 M H_2O_2) + (60 μM complex/IBF)]; lane VII, [DNA + (60 μM complex/IBF)+(2 mM NaN_3)]; lane VIII, [DNA+ (60 μM complex/IBF)] + (2 μL DMSO)]

the basis of the literature available on a particular drug, *viz.* IBF and complexes **1–5** against DU145 (prostate cancer), HCT-15 (colon adenocarcinoma) and Caco-2 (colorectal adenocarcinoma); MESNA and complexes **6–10** against DU145, HCT-15 and HeLa (cervical cancer); and WR, Sul and complexes **11–19** against HCT-15, MCF-7 (mammary cancer), HeLa and LNCaP (androgen-sensitive prostate adenocarcinoma). IC_{50} values for all of the tested compounds along with the reference drugs, *cis*-platin and 5-fluorouracil are listed in Table 3. Calculation of IC_{50} (inhibitory concentration) values was carried out using best linear fit regression model[49,50,53,54] and was an average of two values calculated through two independent experiments. The literature review revealed that the compounds exhibiting IC_{50} < 1.0, 1.0–10.0, 10.0–30.0, >30.0–100.0 and >100.0 μM are considered as highly cytotoxic, considerably cytotoxic, moderately cytotoxic, mildly cytotoxic and non-cytotoxic, respectively.[49] The results indicate that the complexes display different activities against different cell lines. Complex **3** Ph_3Sn(IBF) displayed maximum cytotoxicity towards the colorectal cancer (Caco-2), exhibiting an IC_{50} value (1.21 μM) many fold less than that of *cis*-platin, followed by complex **2** Bu_3Sn(IBF) (IC_{50} = 2.48 μM) and complex **4** {[Me_2Sn(IBF)]$_2$O}$_2$ (IC_{50} = 13.38 μM). All of the complexes (**1–5**) except complex **1** [Me_3Sn(IBF)] induce cytotoxicity among the tested cancer cell lines. Further, IBF indicated potent cytotoxicity only against prostare cancer cells (DU 145) (IC_{50} = 1.65±0.2 μM) and it is non-cytotoxic (IC_{50} 100 μM) against HCT-15 and Caco-2 cell lines. Complexes

TABLE 3 Cytotoxic screening results of organotin complexes of ibuprofen (IBF), MESNA, WR and SUL against the different cell lines of human origin; IC_{50} value is expressed in μM ± SEM.

Drugs/complexes	DU145	HCT-15	Caco-2	MCF-7	HeLa	LNCaP
IBF	1.65±0.2	100	100	–	–	–
1 [(Me_3Sn)(IBF)]	100	100	100	–	–	–
2 [(Bu_3Sn)(IBF)]	100	100	**2.48±0.1**	–	–	–
3 [Ph_3Sn(IBF)]	19.22±0.8	100	***1.21±0.84***	–	–	–
4 {[Me_2Sn(IBF)]$_2$O}$_2$	***3.97±0.81***	**2.188±0.67**	**13.38±1.5**	–	–	–
5 [$Bu_2Sn(IBF)_2$]	**5.92±1.54**	32.32±2.1	100	–	–	–
MESNA	100	100	–	–	100	–
6 [$Me_2Sn(MESNA)_2$]	100	100	–	–	100	–
7 [$Bu_2Sn(MESNA)_2$]	100	100	–	–	100	–
8 [$Oct_2Sn(MESNA)_2$]	100	19.22±0.8	–	–	100	–
9 [$Ph_2Sn(MESNA)_2$]	**11.89±0.6**	**1.69±0.3**	–	–	**3.54±0.2**	–
10 [$Bu_2Sn(MESNA)_2$.Phe]	**7.15±0.7**	***0.83±0.1***	–	–	***1.85±0.4***	–
WR	–	16.2±0.8	–	500	375±25	500
11 ([Me_3Sn(WR)]	–	14.8±3.2	–	Very wide	500	500
12 [Bu_3Sn(WR)])	–	**14.5±0.8**	–	479±16	251±14	500
SUL	–	14.9±0.9	–	406±22	179±30	465±15
13 [Me_3Sn(SULl)]	–	13.8±0.9	–	500	250±15	500
14 [Ph_3Sn(Sul)]	–	**13.2±1.2**	–	500	240±10	Very wide
15 [Bu_3Sn(Sul)]	–	14.4±1.8	–	408±14	157±17	Very wide
16 [$Ph_2Sn(Sul)_2$]	–	15.1±0.6	–	500	500	359±14
17 [$Me_2SnCl(Sul)]_2$	–	16.2±0.4	–	388±10	179±11	Very wide
18 [$Bu_2Sn(Sul)_2$]	–	14.3±0.4	–	301±25	149±16	Very wide
19 [$Oct_2Sn(Sul)_2$	–	14.6±0.8	–	500	Very wide	456±22
5-FU	15.4±0.8	12.2±0.5	–	0.48±0.1[a]	2.08±0.2	–
Cis-platin	–	5.04±1.4[a]	96.38 ± 32.03[b]	13.98±0.4[a]	18[c]	–

MESNA, Sodium 2-mercaptoethanesulfonate; WR (warfarin), 2H-1-benzopyran-2-one,4-hydroxy-3-(3-oxo-1-phenylbutyl), SUL (sulindac), 2-[5-fluoro-1-[(4-methanesulfinylphenyl)methylidene]-2-methyl-1H-inden-3-yl]acetic acid. DU145, Prostate cancer cells; HCT-15, colon adenocarcinoma cells; Caco-2, colorectal adenocarcinoma cells; MCF-7, mammary cancer; HeLa, cervical cancer; and LNCaP, androgen-sensitive prostate adenocarcinoma;

[a]Nath et al.[50]

[b]Nurcahyanti and Wink[51];

[c]Larasati et al.[52](–) Not determined

4 {[Me_2Sn(IBF)]$_2$O}$_2$ and **5** [$Bu_2Sn(IBF)_2$] displayed about 4 to 2.6 times higher activity comapred with 5-fluorouracil in terms of their IC_{50} value against DU 145. Complex **3** was moderately cytotoxic against DU 145. Complex **4** (IC_{50} = 2.188 μM) also displayed maximum cytotoxicity against colon cancer cells (HCT-15), which is around 6 and 2 times higher than 5-fluorouracil and *cis*-platin, respectively. Hence, complex **4** {[Me_2Sn(IBF)]$_2$O}$_2$ is highly cytotoxic and displayed maximum cytotoxicity against prostate and colon cancer cell lines among complexes **1**–**5**, while complex **3** [Ph_3Sn(IBF)] is highly regressive against colorectal cancer cell lines. Complexes **9** [Ph_2Sn(MESNA)] and **10** [$Bu_2Sn(MESNA)_2$·Phen] are highly cytotoxic against DU 145, HCT-15 and HeLa among the organotin-MESNA complexes and complex **8** [$Oct_2Sn(MESNA)_2$] is moderately active only against colon cancer cell lines; however, MESNA and complexes **6** [$Me_2Sn(MESNA)_2$] and **7** [$Bu_2Sn(MESNA)_2$] are non-cytotoxic against all the tested cancer cell lines. Complex **10** exhibited maximum cytotoxicity against colon cancer cells which was followed by complex **9**, which had 6–14 times greater activity compared with *cis*-platin and 5-fluorouracil. Complexes **9** and **10** demonstrated considerably high cytotoxicity (IC_{50} = 7–12 μM) against DU145

cell lines (possessing intrinsic and acquired resistance to *cis*-platin), and also against HeLa (cervical cancer) cell lines, and even greater or comparable activity with 5-fluorouracil and many-fold greater than *cis*-platin. The IC_{50} values listed in Table 3 indicated that WR and SUL as well as their respective complexes **11–19** displayed no cytotoxicity towards MCF-7, HeLa and LNCaP cell lines. Further, WR, SUL and complexes **11–19** were found to induce good cytotoxicity towards colon cancer (HCT-15) cell lines, comparable with 5-fluorouracil, and lesser cytotoxic than *cis*-platin. Complex **14** [Ph_3Sn(SUL)] induced the highest cytotoxic effect against HCT-15 cell lines among organotin–SUL complexes.

Saxena and Huber[55] explained the activity of organotin (IV) complexes on the basis of the availablity of coordination postions around tin metal, the relative stability of the tin–ligand bond and the balance between hydrophilicity and lipophilicity in order to cross the cell membranes. On carefully examining the structure–activity relationship of the tested compounds of a specific drug, the maximum cytotoxicity of Ph_3Sn(IBF) (complex **3**) and Bu_3Sn(IBF) (complex **2**) against colorectal cancer can be explained by their tetrahedral structure and the higher lipophilic behavior of phenyl and butyl groups. Further, the high cytotoxic effect of complex **4**, $\{[Me_2Sn(IBF)]_2O\}_2$, can be explained on the basis of synergistic effect of organotin(IV) moieties present in the tetranuclear complex. Further, high to moderate activity of the octahedral complex **5**, $Bu_2Sn(IBF)_2$ is due to the lesser availability of the coordination positions eventually compensated for by the higher lipophilicity of the butyl moieties.

The presence of 1,10-phenanthroline moiety makes the ligand (MESNA) more labile in complex **10** [$Bu_2Sn(MESNA)_2$·Phen] compared with complex **7** [$Bu_2Sn(MESNA)_2$], which may be responsible for the generation of active metal species. Further, complexes **6** [$Me_2Sn(MESNA)_2$] and **7** [$Bu_2Sn(MESNA)_2$] were more stable towards hydrolysis in buffer solution at physiological pH compared with other complexes,[20] which could explain their low cytotoxicity. Hence, the electronic nature and

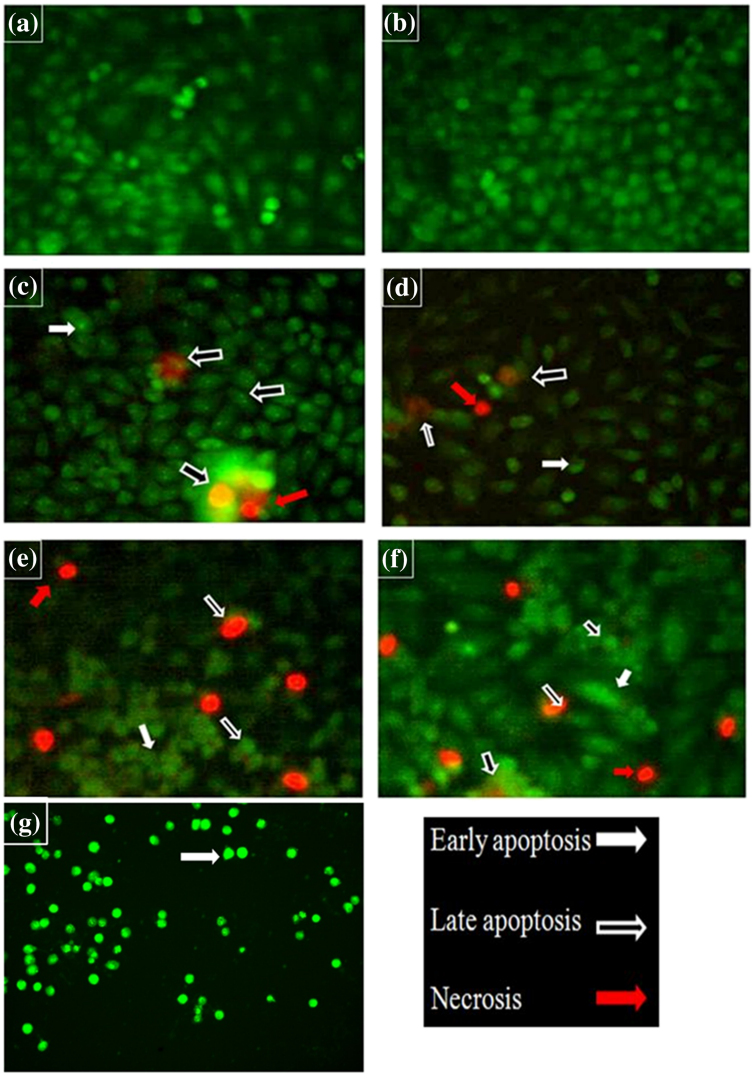

FIGURE 9 AO/EB staining of HCT-15 cell lines: (a) control; (b) vehicle (DMSO) treated cells; (c) cells treated with IC_{50}value of complex **4**; (d) cells treated with IC_{50}value of complex **9**; (e) cells treated with IC_{50}value of complex **10**; and (f) cells treated with IC_{50}value of complex **14**

the balance between hydrophilic and lipophilic characters of the complexes may also be responsible for the difference in their activities.[53] The presence of phenyl and butyl groups in complexes **9** [$Ph_2Sn(MESNA)_2$] and **10** [$Bu_2Sn(MESNA)_2$·Phen], respectively, may be responsible for their remarkable cytotoxicity against the prostate cancer, colon adenocarcinoma and cervical cancer cells.

The studies on the structure–activity relationship of different organotin complexes towards antitumor activity describe how factors like the stability of Sn-heteroatom bond, lipophilic and hydrophilic balance, geometry around the tin atom in the test compounds and the stability of Sn-alkyl and Sn-aryl bonds towards hydrolysis, are important to determine cytotoxicity.[48,55–58] The lesser cytotoxicity of complexes **11-19** can be explained on the basis of the high stability of the Sn–O bond and insufficiency to produce active tin species, i.e. R_2Sn^{2+} and R_3Sn^{+}, responsible for antitumor activity.

From the above-mentioned analysis it is concluded that the metallation of drugs with dibutyl-, diphenyl-, triphenyl- and tributyltin(IV) moieties increases their cytotoxicity and DNA binding capacities many fold. The introduction of 1,10-phenantholine moiety in the organotin–drug complexes increases the *in vitro* antitumor activity of the complexes. [$Bu_2Sn(MESNA)_2$·Phen] displayed the maximum antitumor activity against HCT-15 (IC_{50} = 0.83 μM) and HeLa cell lines (IC_{50} = 1.85 μM) among all of the synthesized complexes. {[$Me_2Sn(IBF)]_2O$}$_2$ displayed the highest antitumor activity against DU145 cancer cell line (3.97 μM) and [(Ph_3Sn)(IBF)] demonstrated the maximum activity against Caco-2 cell lines (1.21 μM). IBF and complexes [$Bu_2Sn(MESNA)_2$·Phen], {[$Me_2Sn(IBF)]_2O$}$_2$ and [(Bu_2Sn)(IBF)$_2$] displayed remarkable cytotoxicities against DU145 cell lines which are resistant to *cis*-platin, hence they can be tested further. It has been analysed that different cell lines displayed different behavior towards similar complexes as far as their cytotoxicities are concerned. Furthermore, the DNA binding ability and DNA cleavage activity of the compounds alone may not describe the

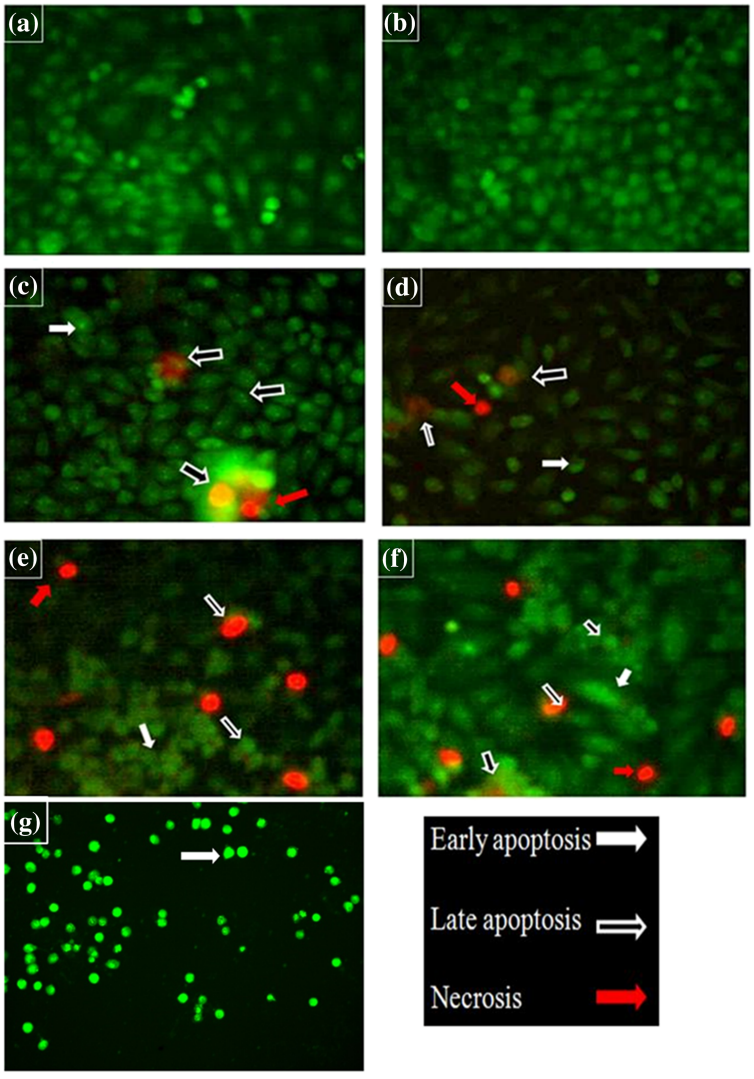

FIGURE 10 AO/EB staining of DU145 cell lines: (a) control; (b) vehicle (DMSO) treated cells; (c) cells treated with IC_{50}value of IBF; (d) cells treated with IC_{50}value of complex **4**; (e) cells treated with IC_{50}value of complex **9**; (f) cells treated with IC_{50}value of complex **10**; and (g) cells treated with IC_{50} value of complex **5**

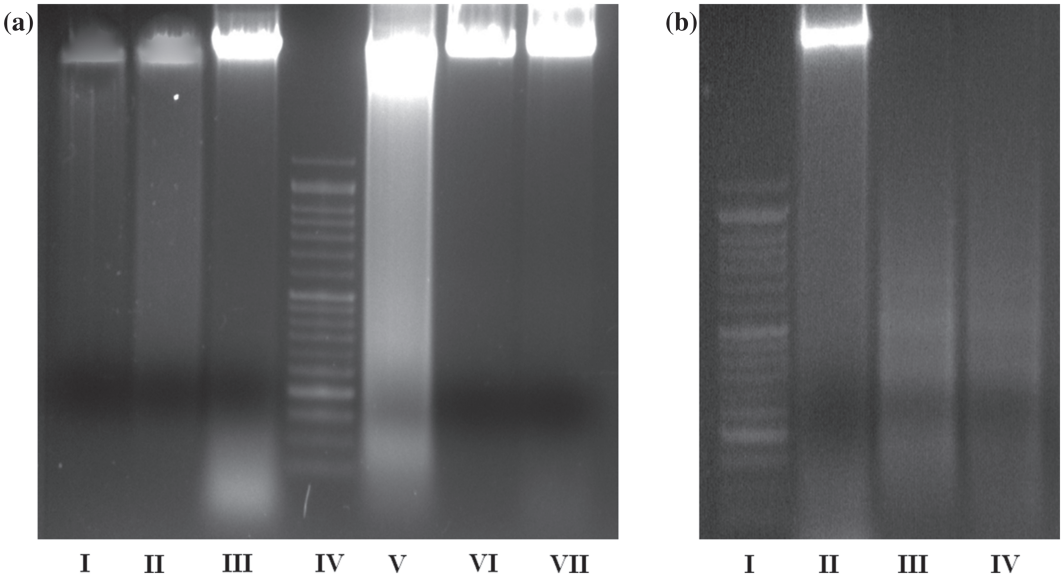

FIGURE 11 Fragmentation pattern of DNA extracted from cell lines on treatment with complexes **4** and **10**, through agarose gel electrophoresis: (a) lane I, control (DNA extracted from DU145); lane II, DNA extracted from DU145 treated with complex **10**; lane III, DNA extracted from DU145 treated with complex **4**; lane IV, DNA marker (50 base pairs); lane V, DNA extracted from HCT-15 treated with complex **4**; lane VI, DNA extracted from HCT-15 treated with complex **10**; and lane VII, control (DNA extracted from HCT-15). (b) lane 1, DNA marker (50 base pairs); lane II, vehicle-treated control (HeLa DNA); lane III, DNA extracted from HeLa treated with complex **4**; and lane IV, DNA extracted from HeLa treated with complex **10**

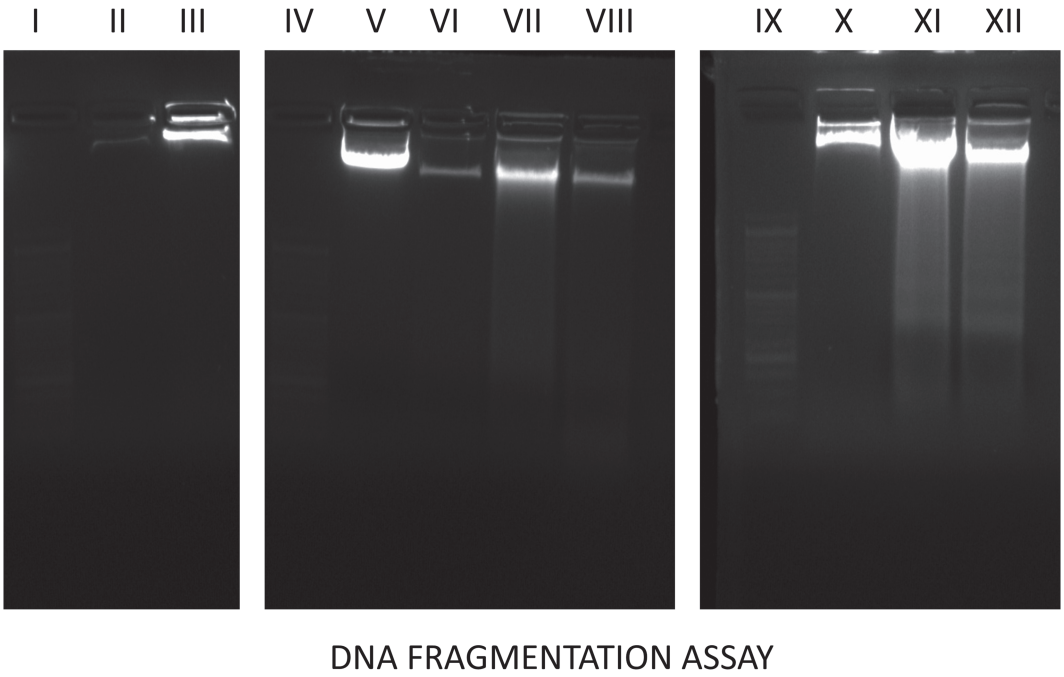

FIGURE 12 Fragmentation pattern of DNA extracted from cell lines on treatment with complexes through agarose gel electrophoresis: lanes I–III, HCT-15 cell line; lanes IV–VIII, DU145 cell line; lanes IX–XII, HeLa cell line. Lane I, DNA marker (50 base pairs); lane II, control (DNA extracted from HCT-15); lane III, DNA extracted from HCT-15 treated with complex **14**; lane IV, DNA marker (50 base pairs); lane V, control (DNA extracted from DU145 cells); lanes VI, VII and VIII, DNA extracted from DU145 treated with complexes **3**, **5** and **9**, respectively; lane IX, DNA marker (50 base pairs); lane X, control (DNA extracted from HeLa); and lanes XI and XII: DNA extracted from HeLa treated with complex **9** and **10**, respectively

antitumor effect of the compounds completely. Therefore, the antitumor activities of the organotin(IV) compounds may be controlled by other factors along with the DNA binding and cleavage abilities. Further experiments are needed in order to explore the cause of cytotoxicity and in-depth mechanisms.

AO/EB staining of cells

This study is an important tool to distinguish between the normal viable cells, early apoptotic cells, late apoptotic cell and necrotic cells. This method is based on the morphological changes that occur in the cytoplasmic membranes and nuclear chromatin material of cells during the process of apoptosis. On the basis of fluorescence emission of AO/EB-stained cells and their chromatin condensation, the cells can be identified as: (a) live/viable cells with intact nuclei which take up AO dye and appear green with uniform structures; (b) early apoptotic cells that can be detected with bright green nuclei with condensed chromatin, but with intact membranes; (c) late apoptotic cells stained with EB that appear orange owing to their ruptured cell membranes and fragmented chromatin material; and (d) necrotic cells with normal nuclei and uniform structures that look like those of viable cells except for the orange-red uniform EB staining.[59] The AO/EB staining of the cancer cells was performed by treating them with the IC_{50} value of the respective test compounds having the highest cytotoxicity towards the particular cell line. The morphological changes appearing in the HCT-15, DU145, Caco-2 and HeLa cells when treated with inhibitory concentration (IC_{50}) of IBF and complexes **2**, **4**, **5**, **9** **10** and **14** are illustrated in Figs 9, 10, S18 and S19.

In the control (untreated) and vehicle control (treated with DMSO) all of the cells appear uniform with green fluorescing nuclei; however, in the case of HCT-15 cell lines treated with complexes **4**, **9**, **10** and **14**, Caco-2 cell lines treated with complex **2**, DU145 cell lines treated with IBF and complexes **4**, **5**, **9** and **10**, and HeLa cell lines treated with complexes **9** and **10**, cells appear green with condensed chromatin indicating early apoptotic cells and orange to red coloured cells with the condensed or fragmented chromatin material indicating the late apoptosis. Further, a very small amount of necrosis was also found in all of the stained cell lines treated with almost all complexes. Hence, both the apoptosis (majorly) and necrosis are responsible for the cytotoxicity of the complexes.

DNA fragmentation assay

DNA fragmentation assay is regarded as the hallmark of apoptosis. During apoptosis, Caspase-3 triggers the endonulcease activity which cleaves the DNA at the internucleosomal units (where DNA is not wrapped by the histones) and results in the fragmentation of DNA into

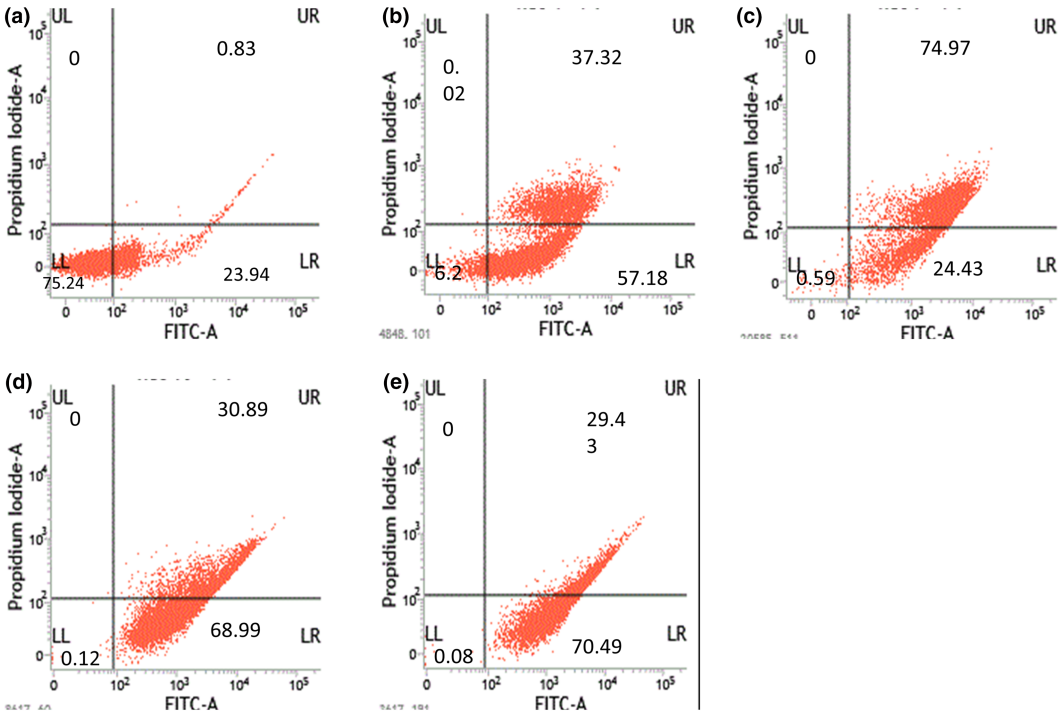

FIGURE 13 Flow cytometric analysis of apoptosis in HCT-15cells: (a) the vehicle-treated control cells (HCT-15); (b–e) complexes **4**, **9**, **10** and **14** treated HCT-15 cells, respectively, for a period of 24 h. UL (upper left), necrotic cells; UR (upper right), late apoptotic cells; LL (lower left), viable cells; LR (lower right), early apoptotic cells

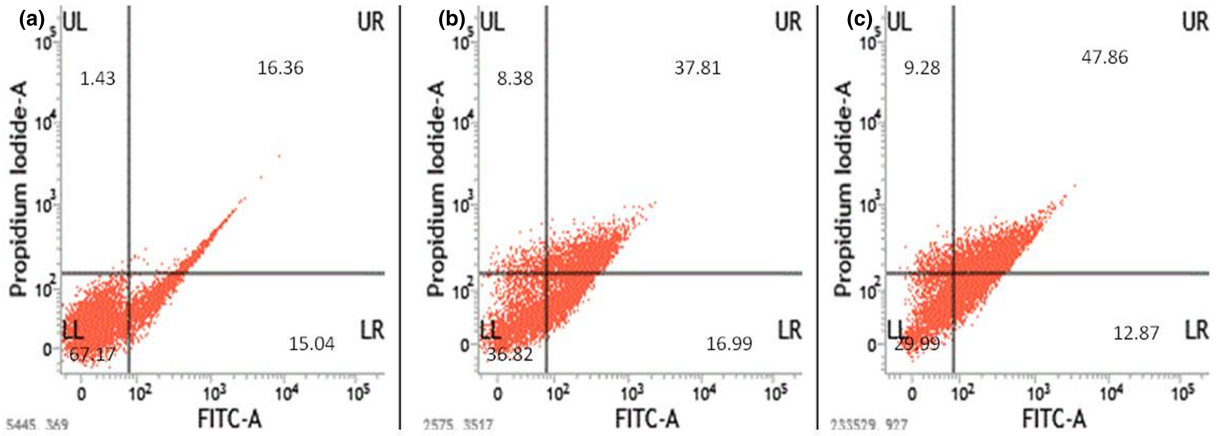

FIGURE 14 Flow cytometric analysis of apoptosis in Hela cells; (a) the vehicle-treated control cells; (b and c) complex **9** and **10** treated cells, respectively, for a period of 24 h. UL (upper left), necrotic cells; UR (upper right), late apoptotic cells; LL (lower left), viable cells; LR (lower right), early apoptotic cells

different oligomer units, which look like a DNA ladder when subjected to agarose gel electrophoresis.[60] In contrary to apoptotic activity, necrosis leads to the appearance of irregular-sized DNA bands or DNA smear in agarose gel electrophoresis. However, in some cases single-strand cleavage in DNA has been observed in apoptotic phenotypes, which does not form the DNA ladder in gel electrophoresis.[61] In the present study the DNA (extracted from the DU145 and HCT-15 cells) treated with complexes **4** $\{[Me_2Sn(IBF)]_2O\}_2$ and **10** $[Bu_2Sn(MESNA)_2{\cdot}Phen]$ and

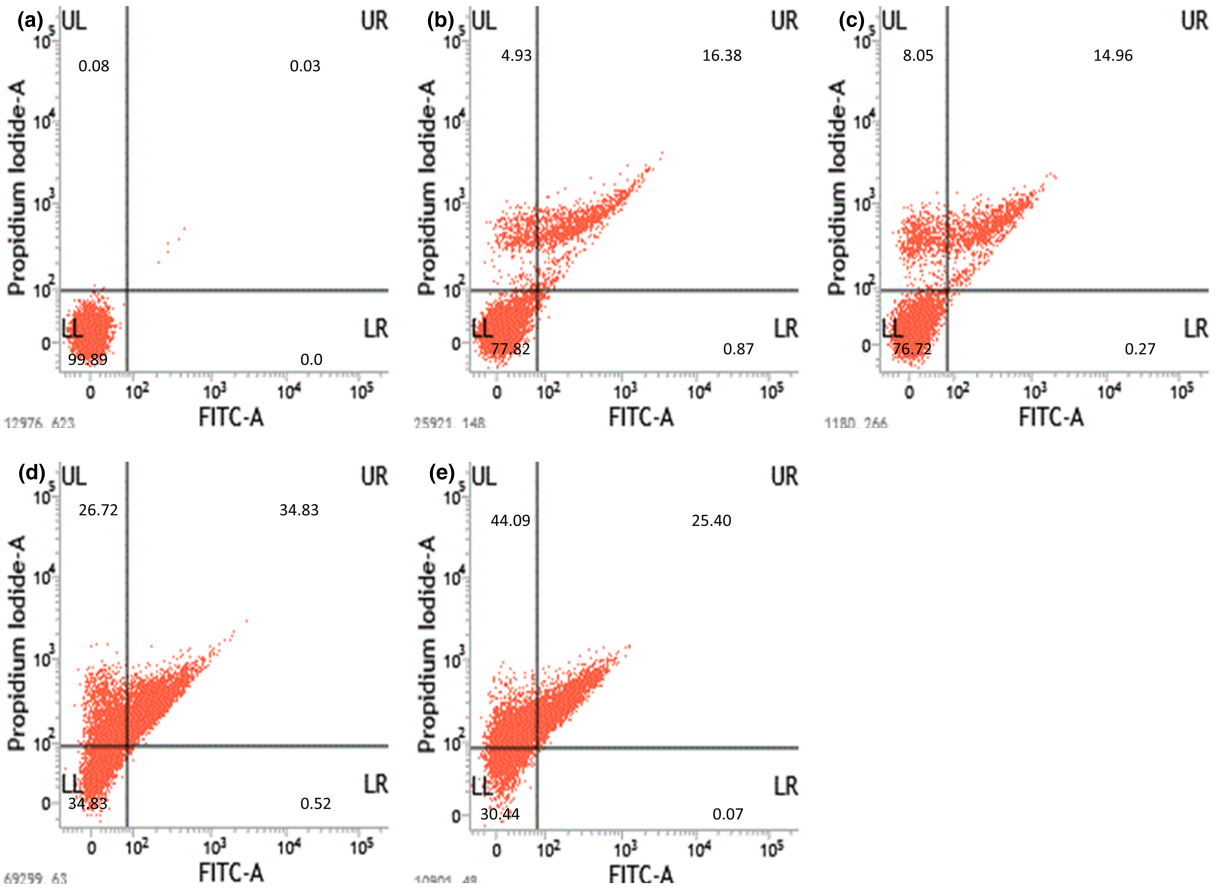

FIGURE 15 Flow cytometric analysis of apoptosis in DU145 cells; (a) the vehicle-treated control cells; (b–e) complex **4**, **5**, **9 and 10** treated cells, respectively, for a period of 24 h. UL (upper left), necrotic cells; UR (upper right), late apoptotic cells; LL (lower left), viable cells; LR (lower right), early apoptotic cells

HCT-15 cells treated with complex **14** does not reveal any fragmentation and looks similar to that of the vehicle-treated DNA control [Figs 11(a) and 12], which means that apoptosis (as shown in AO/EB staining) and cytotoxicity caused by these complexes against DU145 and HCT-15 are caused by the methods other than the Caspase-3 activated DNA fragmentation. This may be either due to the single-strand scission of the DNA or other changes occurring on the cell surface. Furthermore, a ladder formation is seen [Fig. 11(b)] in the fragmentation pattern of DNA extracted from HeLa cells, when treated with the complexes **4** and **10** and DNA extracted from Du 145 and HeLa treated with complexes **3**, **5**, **9** and **9**, **10**, respectively (Fig. 12), indicating apoptosis as the main cause of cytotoxicity in Du 145 and HeLa cell lines.

Flow cytometry for analysis of apoptosis

To verify whether the cytotoxic effect of complexes **4**, **9**, **10** and **14** on HCT-15 cells, complexes **9** and **10** on HeLa cells and complexes **4**, **5**, **9** and **10** on DU 145 cells was due to apoptosis (programe cell death) induction, the flow cytometry analysis was performed and the results are shown in Figs 13–15. The observed results clearly indicated enhanced apoptosis, i.e. mostly late apoptosis, lower to medium level of early apoptosis and very small necrosis events occuring in the complexes treated cells as compared with the vehicle-treated cells. The quantification of cell population revealed that, as compared with the control cells, the treated cells with complexes **4**, **9**, **10** and **14** on HCT-15 cells (Fig. 13) showed significant early apoptotic cell death: around 57.18, 24.43, 68.99 and 70.49%, and late apoptotic cell death around 37.32, 74.97, 30.89 and 29.4%, respectively. Complex **9** showed maximum late apoptosis. However, cells treated with complex **4** showed insignificant necrotic cell death (0.02%). Therefore, we can conclude that the cytotoxic effect of the studied complexes on HCT-15 cells was due to the induction of apoptosis (both early and late) in the cells.

The quantification of cell population as compared with the control cells in Fig. 14 revealed that the cells treated with complexes **9** and **10** on HeLa cells also exhibited significant late apoptotic cell death, around 37.81and 47.86%, and less early apoptotic cell death, around 16.99 and 12.87%, respectively. However, a small amount of necrotic cell death (8.38–9.28%) was also observed. Therefore, the cytotoxic effect of complexes **9** and **10** on HeLa cells was majorly due to the induction of apoptosis (both early and late) and necrosis also played a minor role leading to the cell death, whereas the case of DU145 cells treated with complexes **4**, **5**, **9** and **10** (Fig. 15) indicated late apoptotic cell death around 16.38, 14.96, 34.83 and 25.40% and necrotic cell death around 4.93, 8.05, 26.72 and 44.09% with an insignificat amount of early apoptotic cell death (0.07–0.87%). Therefore, both apoptosis and necrosis are responsible for the cytotoxicity of the studied complexes on DU 145 and maximum necrosis is observed in complex **10**-treated cells.

4 | CONCLUSIONS

Since the role of the anti-inflammatory drugs in the combination chemotherapy with other antitumor drugs is a well-known fact, we were eager to explore the effect of combination of organotin(IV) moieties with a very simple and well-known NSAID, IBF, which is initiated by a successful syntheses of di- and triorganotin(IV) complexes of IBF. The single-crystal X-ray determination of $[Ph_3Sn(IBF)]$ revealed an intermediate geometry (between Td and TBP geometries) around tin with bidentate mode of carboxylate group. A distannoxane structure for $\{[Me_2Sn(IBF)]_2O\}_2$ and a highly distorted octahedral structure or tetrahedral bicapped structure with two carboxylate groups coordinating through bidentate mode were proposed for $[(Bu_2Sn)(IBF)_2]$, which were further validated through DFT calculations in a gaseous state. However, these complexes lose the bidentate mode of coordination of carboxylate in solution state as revealed by multinuclear NMR studies. DNA binding studies and viscosity measurement of DNA depicted the intercalation of IBF and $[(Bu_2Sn)(IBF)_2]$ within the base pairs of DNA; however, external binding (electrostatic or groove binding) was revealed for complexes **1** and **2**. Further, DNA cleavage activity specified them as potential DNA cleaving agents, which displayed a concentration-dependent cleavage of DNA. A hydrolytic mechanism of cleavage was revealed for IBF and complexes except complex **1**, although the involvement of reactive oxygen radical in the cleavage activity could not be ruled out.

Furthermore, the *in vitro* cytotoxicity studies for currently synthesized complexes **1–5** and already synthesized organotin–drug complexes highlighted the highly cytotoxic effect of complexes **3**, **4**, **5**, **9** and **10** against DU145 (prostate cancer), HCT-15 (colon adenocarcinoma), Caco-2 (colorectal adenocarcinoma) and HeLa (cervical cancer) cell lines. Complexes **2** and **3** demonstrated a remarkable cytotoxicity towards Caco-2 (IC_{50} = 1.21 and 2.48 μM, respectively) which is 4–8 times more than that of *cis*-platin. Complexes **4**, **5** and **10** displayed a high cytotoxicity against DU145 (IC_{50} values 3.97, 5.92 and 7.15 μM, respectively), which is resistant to *cis*-platin. Furthermore, complexes **4**, **9** and **10** are highly active (IC_{50} values are 1.88, 1.69 and 0.83μM, respectively) against HeLa cells. The higher activities of $[Bu_3Sn(IBF)]$ and $[(Ph_3Sn)(IBF)]$ complexes against colorectal cancer can be explained on the basis of their tetrahedral structure and

higher lipophilic nature of the butyl and phenyl groups. Further, the cytotoxicity of complex **4**, $\{[Me_2Sn(IBF)]_2O\}_2$, can be described by the synergistic effect of oragnotin (IV) moieties owing to the tetranuclear complex structure. The prostate cancer cell line (DU145) is resistant towards *cis*-platin, hence these complexes can be further studied in order to make them suitable for clinical trials. It was evidenced by the AO/EB staining of the cells, DNA fragmentation assay and flow cytometry assay that the major cause of cell death is apoptosis; however, necrosis in DU 145 cells could not be excluded. A number of commercially used antitumor drugs, i.e. doxorubicin, 5-fluorouracil, *cis*-platin and cladribine, exhibit necrotic and apoptotic effects together. It is concluded that the organotin(IV) complexes exert their cytotoxic effects owing to their dual capability of inducing apoptosis to a greater extent and necrosis to a minor extent.

ACKNOWLEDGEMENTS

The author Ms. R. Kumari is thankful to the Ministry of Human Resources Development (grant no. MHRD -02-23-104-429), India, for the award of Junior/Senior Research Fellowship.

CONFLICT OF INTEREST

The authors declare that they have no competing interest.

ORCID

Mala Nath https://orcid.org/0000-0003-1158-2520

REFERENCES

[1] J. Michael, S. Thun, J. Henley, C. Patrono, *J. Natl Cancer Inst.* **2002**, *94*, 252.

[2] T. Elsaman, M. M. Ali, *Am. J. Res. Comm.* **2016**, *4*(4). www.usa.journals.com.

[3] H. Endo, M. Yano, Y. Okumura, H. Kido, *Cell Death Dis.* **2014**, *5*, e1027.

[4] B. A. Thicher, T. T. Korbut, K. Menon, S. A. Holden, G. Ara, *Cancer Chemother. Pharmacol.* **1994**, *33*, 515.

[5] X. Qu, A. Allan, G. Chui, T. J. Hutchings, P. Jiao, L. Johnson, W. Y. Leung, P. K. Li, G. R. Steel, A. S. Thompson, M. D. Threadgill, T. J. Woodman, M. D. Lloyd, *Biochem. Pharmacol.* **2013**, *86*, 1621.

[6] P. Matos, P. Jordan, *Curr. Pharm. Des.* **2015**, *21*, 2978.

[7] M. A. Husain, S. Ur Rehman, H. M. Ishqi, T. Sarwar, M. Tabish, *RSC Adv.* **2015**, *5*, 64335.

[8] M. A. Husain, T. Sarwar, S. Ur Rehman, H. M. Ishqi, M. Tabish, *Phys. Chem. Chem. Phys.* **2015**, *17*, 13837.

[9] A. T. M. Fiori, W. R. Lustri, A. Magalhães, P. P. Corbi, *Inorg. Chem. Commun.* **2011**, *14*, 738.

[10] C. Núñez, A. Fernández-Lodeiro, J. Fernández-Lodeiro, J. Carballo, J. L. Capelo, C. Lodeiro, *Inorg. Chem. Commun.* **2014**, *45*, 61.

[11] I. M. P. Silva, D. M. de Profirio, R. E. F. de Paiva, M. Lancellotti, A. L. B. Formiga, P. P. Corbi, *J. Mol. Struct.* **2013**, *1049*, 1.

[12] S. R. A. Rico, A. Z. Abbasi, G. Ribeiro, T. Ahmed, X. Y. Wu, D. O. de Silva, *Nanoscale* **2017**, *9*, 10701.

[13] S. Kumar, S. Garg, R. P. Sharma, P. Venugopalan, L. Tenti, V. Ferretti, L. Nivelle, M. Tarpinc, E. Guillon, *New J. Chem.* **2017**, *41*, 8253.

[14] S. Shahzadi, K. Shahid, S. Ali, M. Mazhar, A. Badshah, E. Ahmed, A. Malik, *Turk. J. Chem.* **2005**, *29*, 273.

[15] A. Jalal, S. Shahzadi, K. Shahid, S. Ali, A. Badshah, M. Mazhar, K. M. Khan, *Turk. J. Chem.* **2004**, *28*, 629.

[16] L. Pellerito, L. Nagy, *Coord. Chem. Rev.* **2002**, *224*, 111.

[17] S. Tabassum, S. Mathur, F. Arjmand, K. Mishrab, K. Banerjee, *Metallomics* **2012**, *4*, 205.

[18] T. A. K. Al-Allaf, L. J. Rashan, A. Stelzner, D. R. Powell, *Appl. Organomet. Chem.* **2003**, *17*, 891.

[19] M. Sirajuddin, S. Ali, A. Badshah, *J. Photochem. Photobiol. B, Biol.* **2013**, *124*, 1.

[20] R. Kumari, M. Nath, *Appl. Organometal. Chem.* **2018**, e4365.

[21] R. Kumari, M. Nath, *Appl. Organometal. Chem.* **2017**, e3661. https://doi.org/10.1002/aoc.3661

[22] R. Kumari, M. Nath, *Inorg. Chem. Commun.* **2018**, *95*, 40.

[23] A. Altomare, G. Cascarano, C. Giacovazzo, A. Guagliardi, M. C. Burla, G. Polidori, M. Camalli, *J. Appl. Crystallogr.* **1994**, *27*, 435.

[24] G. Sheldrick, *SHELX-97, program for the solution and refinement of crystal structures*, University of Göttingen, Germany **1997**.

[25] D. Wlodkowic, J. Skommer, Z. Drazynkiewicz, Flow cytometry-based apoptosis detection, in *Methods in Molecular Biology*, (Eds: P. Erhardt, A. Toth) Vol. 559, Humana Press, Totowa, NJ **2009** 19.

[26] M. Nath, P. Roy, R. Mishra, M. Thakur, *Appl. Organomet. Chem.* **2018**, *33*, e4663.

[27] T. P. Lockhart, W. F. Manders, *Inorg. Chem.* **1986**, *25*, 892.

[28] T. P. Lockhart, W. F. Manders, J. J. Zuckerman, *J. Am. Chem. Soc.* **1985**, *107*, 4547.

[29] W. Mao, K. Bao, Y. Feng, Q. Wang, J. Li, Z. Fan, *Main Group Met. Chem.* **2015**, *38*, 27.

[30] A. S. Sougoule, X. Xiao, C. A. Balde, A. M. Sakho, D. Zhu, *Heteroatom Chem.* **2015**, *26*, 270.

[31] F. A. Shah, S. Sabir, K. Fatima, S. Ali, I. Qadri, C. Rizzoli, *Dalton Trans.* **2015**, *44*, 10467.

[32] Mridula, M. Nath, *J. Photochem. Photobiol. B Biol.* **2016**, *162*, 348.

[33] G. K. Sandhu, N. Sharma, E. R. T. Tiekink, *J. Organomet. Chem.* **1991**, *403*, 119.

[34] M. M. Amini, A. Azadmeher, H. R. Khavasi, S. W. Ng, *J. Organomet. Chem.* **2007**, *692*, 3922.

[35] F. A. Shah, K. Fatima, S. Sabir, S. Ali, I. Qadri, N. ud Din, *J. Photochem. Photobiol. B Biol.* **2016**, *154*, 99.

[36] T. S. B. Baul, C. Masharing, S. Basu, E. Rivarola, M. Holčapek, R. Jirásko, A. Lyčka, D. de Vos, A. Linden, *J. Organomet. Chem.* **2006**, *691*, 952.

[37] C. S. Parulekar, V. K. Jain, T. Kesavadas, E. R. T. Tiekink, *J. Organomet. Chem.* **1990**, *387*, 163.

[38] Y. Y. Zhang, R. F. Zhang, S. L. Zhang, S. Cheng, Q. L. Li, C. L. Ma, *Dalton Trans.* **2016**, *45*, 8412.

[39] C. Vatsa, V. K. Jain, T. Kesavadas, E. R. T. Tiekink, *J. Organomet. Chem.* **1991**, *408*, 157.

[40] T. P. Lockhart, J. C. Calabrese, F. David, *Organometals* **1987**, *6*, 2419.

[41] M. J. Frisch, G. W. Trucks, H. B. Schlegel, G. E. Scuseria, M. A. Robb, J. R. Cheeseman, G. Scalmani, V. Barone, B. Mennucci, G. A. Petersson, H. Nakatsuji, M. Caricato, X. Li, H. P. Hratchian, A. F. Izmaylov, J. Blno, G. Zheng, J. L. Sonnenberg, M. Hada, M. Ehara, K. Toyota, R. Fukuda, J. Hasegawa, M. Ishida, T. Nakajima, Y. Honda, O. Kitao, H. Nakai, T. Vreven, J. A. Montgomery, J. E. Peralta Jr., F. Ogliaro, M. Bearpark, J. J. Heyd, E. Brothers, K. N. Kudin, V. N. Staroverov, R. Kobayashi, J. Normand, K. Raghavachari, A. Rendell, J. C. Burant, S. S. Iyengar, J. Tomasi, M. Cossi, N. Rega, J. M. Millam, M. Klene, J. E. Knox, J. B. Cross, V. Bakken, C. Adamo, J. Jaramillo, R. Gomperts, R. E. Stratmann, O. Yazyev, A. J. Austin, R. Cammi, C. Pomelli, J. W. Ochterski, R. L. Martin, K. Morokuma, V. G. Zakrzewski, G. A. Voth, P. Salvador, J. J. Dannenberg, S. Dapprich, A. D. Daniels, Ö. Farkas, J. B. Foresman, J. V. Ortiz, J. Cioslowski, D. J. Fox, *Gaussian 09, (Revision A.02)*, Gaussian, Inc., Wallingford, CT **2009**.

[42] F. Arjmand, A. Jamsheera, *Spectrochim. Acta A* **2011**, *78*, 45.

[43] S. Dey, S. Sarkar, H. Paul, E. Zangrando, P. Chattopadhyay, *Polyhedron* **2010**, *29*, 1583.

[44] X. L. Li, Y. J. Hu, H. Wang, B. Q. Yu, H. L. Yue, *Biomacromolecules* **2012**, *13*, 873.

[45] D. Sahoo, P. Bhattacharya, S. Chakravorti, *J. Phys. Chem. B* **2010**, *114*, 2044.

[46] K. Karidi, A. Garoufis, A. Tsipis, N. Hadjiliadis, H. den Dulk, J. Reedijk, *Dalton Trans.* **2005**, 1176.

[47] S. Tabassum, A. Asim, R. A. Khan, F. Arjmand, D. Rajakumar, P. Balaji, M. A. Akbarsha, *RSC Adv.* **2015**, *5*, 47439.

[48] P. P. Silva, W. Guerra, J. N. Silveira, A. M. da, C. Ferreira, T. Bortolotto, F. L. Fischer, H. Terenzi, A. Neves, E. C. Pereira-Maia, *Inorg. Chem.* **2011**, *50*, 6414.

[49] M. Nath, M. Vats, P. Roy, *Med. Chem. Res.* **2015**, *24*, 51.

[50] M. Nath, M. Vats, P. Roy, *Eur. J. Med. Chem.* **2013**, *59*, 310.

[51] A. D. R. Nurcahyanti, M. Wink, *Peer J.* **2016**. https://doi.org/10.7717/peerj.1542

[52] Y. A. Larasati, D. D. P. Putri, R. Y. Utomo, A. Hermawan, E. Meiyanto, *J. Appl. Pharm.* **2014**, *4*, 14.

[53] M. Nath, M. Vats, P. Roy, *J. Photochem. Photobiol. B Biol.* **2015**, *148*, 88.

[54] M. J. Moshi, E. Innocent, J. J. Magadula, D. F. Otieno, A. Weisheit, P. K. Mbabazi, R. S. O. Nondo, *Tanz. J. Health Res.* **2010**, *12*, 63.

[55] A. K. Saxena, F. Huber, *Coord. Chem. Rev.* **1989**, *95*, 109.

[56] M. Nath, S. Pokharia, G. Eng, X. Song, A. Kumar, *Eur. J. Med. Chem.* **2005**, *40*, 289.

[57] M. Nath, S. Pokharia, X. Song, G. Eng, M. Gielen, M. Kemmer, M. Biesemans, R. Willem, D. De Vos, *Appl. Organomet. Chem.* **2003**, *17*, 823.

[58] R. Barbieri, G. Ruisi, G. Atassi, *J. Inorg. Biochem.* **1991**, *41*, 25.

[59] M. Leite, M. Quinta-Costa, P. S. Leite, J. E. Guimarães, *Anal. Cell. Pathol.* **1999**, *19*, 139.

[60] D. Matassov, T. Kagan, J. Leblanc, M. Sikorska, Z. Zakeri, Measurement of apoptosis by DNA fragmentation, in *Apoptosis Methods and Protocols*, (Ed: H. J. M. Brady), Humana Press, Totowa, NJ **2004**.

[61] D. L. Tomei, P. J. Shapiro, O. F. Cope, *Proc. Natl Acad. Sci.* **1993**, *90*, 853.

SUPPORTING INFORMATION

Additional supporting information may be found online in the Supporting Information section at the end of the article.

How to cite this article: Kumari R, Banerjee S, Roy P, Nath M. Organotin(IV) complexes of NSAID, ibuprofen, X-ray structure of $Ph_3Sn(IBF)$, binding and cleavage interaction with DNA and *in vitro* cytotoxic studies of several organotin complexes of drugs. *Appl Organometal Chem*. 2019; e5283. https://doi.org/10.1002/aoc.5283